AD-A062 391 STEVENS INST OF TECH HOBOKEN N J F/G 13/10
WAVEMETER DATA REDUCTION METHOD AND INITIAL DATA FOR THE SL-7 C--ETC(U)
JUN 78 J F DALZELL N00024-74-C-5451

UNCLASSIFIED SSC-278 NL

| OF |
ADA
062391

END
DATE FILMED
3-79
DDC

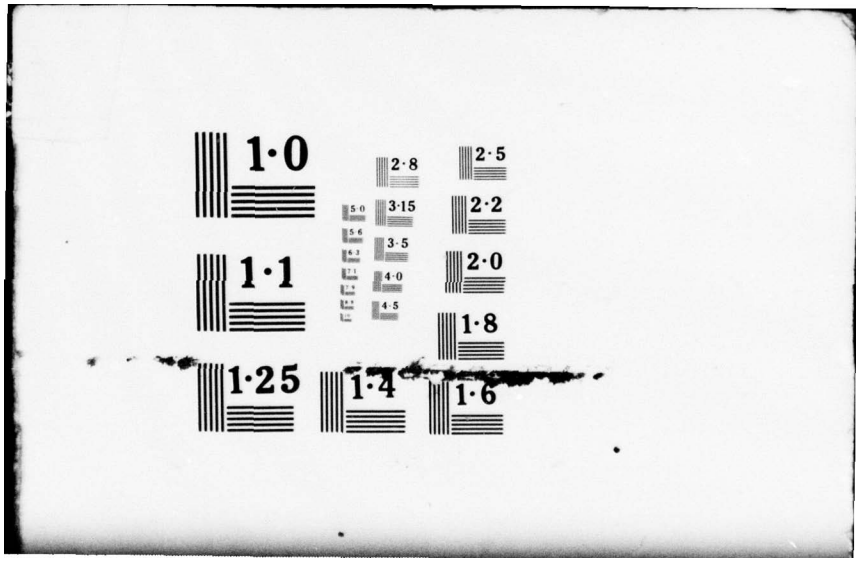
1·0
1·1
1·25
1·4
1·6
1·8
2·0
2·2
2·5
2·8
3·15
3·5
4·0
4·5
5·0
5·6

SSC-278

(SL-7-15)

LEVEL II

# WAVEMETER DATA REDUCTION METHOD AND INITIAL DATA FOR THE SL-7 CONTAINERSHIP





SHIP STRUCTURE COMMITTEE

1978

Member Agencies:
*United States Coast Guard*
*Naval Sea Systems Command*
*Military Sealift Command*
*Maritime Administration*
*United States Geological Survey*
*American Bureau of Shipping*

**Ship Structure Committee**

An Interagency Advisory Committee
Dedicated to Improving the Structure of Ships

Address Correspondence to:
*Secretary, Ship Structure Committee*
*U.S. Coast Guard Headquarters,(G-M/82)*
*Washington, D.C. 20590*

SR-1221

**SEP 1978**

This report is one of a group of Ship Structure Committee Reports which describes the SL-7 Instrumentation Program. This program, a jointly funded undertaking of Sea-Land Service, Inc., the American Bureau of Shipping and the Ship Structure Committee, represents an excellent example of cooperation between private industry, regulatory authority and government. The goal of the program is to advance understanding of the performance of ships' hull structures and the effectiveness of the analytical and experimental methods used in their design. While the experiments and analyses of the program are keyed to the SL-7 Containership and a considerable body of the data developed relates specifically to that ship, the conclusions of the program will be completely general, and thus applicable to any surface ship structure.

The program includes measurement of hull stresses, accelerations and environmental and operating data on the S.S. Sea-Land McLean, development and installation of a microwave radar wavemeter for measuring the seaway encountered by the vessel, a wave tank model study and a theoretical hydrodynamic analysis which relate to the wave induced loads, a structural model study and a finite element structural analysis which relate to the structural response, and installation of long term stress recorders on each of the eight vessels of the class. In addition, work is underway to develop the initial correlations of the results of the several program elements.

Results of each of the program elements are being made available through the National Technical Information Service, each identified by an SL-7 number and an AD- number. A list of all SL-7 reports available to date is included in the back of this report.

This report contains an analysis of the radar wavemeter and the Tucker wavemeter systems installed on the Sea-Land McLean. Improvements in the systems are discussed for future applications. The data presentation procedure to be used in subsequent reports is discussed.

Henry H. Bell
**Rear Admiral, U.S. Coast Guard**
**Chairman, Ship Structure Committee**

SSC-278

(SL-7-15)

(9) TECHNICAL REPORT,

on

Project SR-1221

"Correlation and Verification of

Wavemeter Data from the SL-7"

(6) WAVEMETER DATA REDUCTION METHOD AND INITIAL DATA FOR THE SL-7 CONTAINERSHIP

by

(10) J. F. Dalzell

Stevens Institute of Technology

under

Department of the Navy
Naval Ship Engineering Center
Contract No. (15) N00024-74-C-5451



(11) Jun 78

(12) 81p.

(18) SSC, SSC

(19) 278, SL-7-15



U. S. Coast Guard Headquarters
Washington, D.C.
1978

## ABSTRACT

So that more precise correlations between full scale observations and analytical and model results could be carried out, one of the objectives of the instrumentation program for the SL-7 class container ships was the provision of instrumental measures of the wave environment. To this end, two wave meter systems were installed on the S.S. SEA-LAND McLEAN. Raw data was collected from both systems during the second (1973-1974) and third (1974-1975) winter data collecting seasons.

It was the purpose of the present work to reduce this raw data, to develop and implement such corrections as were found necessary and feasible, and to correlate and evaluate the final results from the two wave meters. In carrying out this work it was necessary to at least partly reduce several other channels of recorded data, so that, as a by-product, reduced results were also obtained for midship bending stresses, roll, pitch, and two components of acceleration on the ship's bridge.

As the work progressed it became evident that the volume of documentation required would grow beyond the usual dimensions of a single technical report. For this reason the analyses, the methods, the detailed results, discussions, and conclusions are contained in a series of ten related reports.

This report documents some background analyses, as well as those which were necessary to develop the needed corrections to the raw digitized data. Implementation of the results of the various analyses in a second data reduction stage is discussed.


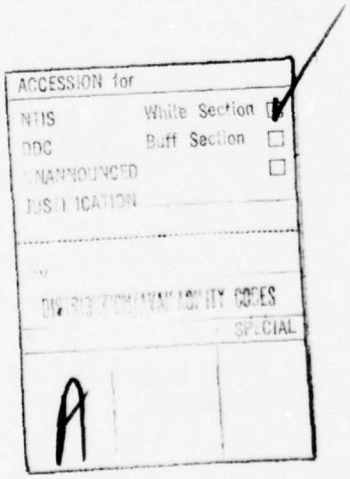

CONTENTS


| | page |
|---|---|
| INTRODUCTION | 1 |
| BACKGROUND | 1 |
| PRELIMINARY DISCUSSION | 2 |
| Overall Limitations and Goals | 2 |
| ANALYSIS OF THE RADAR WAVE HEIGHT SYSTEM | 4 |
| General Analysis | 4 |
| Axis System | 8 |
| Expansion of the Slant Range Vector | 11 |
| Expansion of Radar Position Vector | 11 |
| The Vertical Component of Acceleration | 14 |
| Relationship Between Ideal Pendulum Transducer Outputs and Euler Angles | 16 |
| Approximations to the Required Functions of Roll and Pitch Angles | 18 |
| Error Analysis: Pendulum Transducers | 21 |
| Correction of Radar Range for Vertical Motion of the Ship | 29 |
| The Low Frequency Cut-Off | 31 |
| Filtering Methods - Sampled Data | 36 |
| Preliminary Numerical Development; Fast Convolution Method | 38 |
| Radar Wave Processing System | 39 |
| Simulation of Data for Final Development of Low Frequency Cutoff Parameters of $H(\omega_e)$ | 41 |
| Final Version of the Low Frequency Cutoff Parameters | 42 |
| Results of Final Precision Checks | 44 |
| Sample Evaluation with Actual Data | 47 |
| Retrospective | 52 |
| ANALYSIS OF THE TUCKER METER | 54 |
| Background | 54 |
| The SL-7 Tucker Meter Installation | 56 |
| Analysis of Possible Corrections | 57 |
| A Study of Errors Induced by Double Integration | 57 |

page

INDIRECT METHODS OF WAVE MEASUREMENT . . . . . 67

THE FINAL DATA REDUCTION AND PRESENTATION PROCEDURE . . . . . 69

REFERENCES . . . . . 75

LIST OF FIGURES


| | | PAGE |
|---|---|---|
| 1 | OVERALL GEOMETRY - RADAR | 6 |
| 2 | SEMI-FIXED AND MOVING AXIS SYSTEMS (NO HEAVE OR SWAY) | 10 |
| 3 | RADAR AIMING NOTATION | 12 |
| 4 | RELATIVE POSITIONS OF ACCELEROMETERS AND RADAR | 12 |
| 5a | SAMPLE TIME HISTORY, RUN 401 | 26 |
| 5b | SAMPLE TIME HISTORY, RUN 401 | 26 |
| 6 | LOCATION OF INTEGRATION ERRORS IN THE WAVE FREQUENCY/HEADING PLANE, SHIP SPEED 20 KT. | 30 |
| 7 | LOCATION OF INTEGRATION ERRORS IN THE WAVE FREQUENCY/HEADING PLANE, SHIP SPEED 30 KT. | 30 |
| 8 | LOCATION OF INTEGRATION ERRORS FOR QUARTERING/ FOLLOWING SEAS IN THE WAVE LENGTH - HEADING PLANE | 30 |
| 9 | DEFINITION OF $H(w_e)$ | 39 |
| 10 | PRECISION OF DOUBLE INTEGRATION BY FAST CONVOLUTION METHODS (HARMONIC AND NARROW BAND ACCELERATION) | 41 |
| 11 | PRECISION OF DOUBLE INTEGRATION BY FAST CONVOLUTION METHODS (WIDE BAND ACCELERATION) | 41 |
| 12a | SAMPLE RANGE, ACCELERATION, DISPLACEMENT, AND ENCOUNTERED WAVE TIME HISTORIES, RUN 401 | 43 |
| 12b | SAMPLE RANGE, ACCELERATION, DISPLACEMENT, AND ENCOUNTERED WAVE TIME HISTORIES, RUN 401 | 43 |
| 13 | RUN 401, RADAR WAVE SPECTRUM AND COMPONENTS | 45 |
| 14 | COMPARISON OF NOMINAL MIDSHIP MOMENT RESPONSE FROM SPECTRAL RATIO WITH MODEL DATA (RUN 401) | 47 |
| 15 | DIAGRAM OF THE TUCKER METER INSTALLATION | 53 |
| 16a | RUN 401, SAMPLE TIME HISTORIES, TUCKER METER AND MEAN DYNAMIC HEAD | 58 |
| 16b | RUN 401, SAMPLE TIME HISTORIES, TUCKER METER AND MEAN DYNAMIC HEAD | 58 |
| 17 | SPECTRA DERIVED FROM TUCKER DATA (RUN 401) | 58 |
| 18 | RUN 401 -- VOYAGE 32W -- TAPE 145 -- INDEX 17 -- INTERVAL 1 | 63 |
| 19 | RUN 401 -- VOYAGE 32W -- TAOE 145 -- INDEX 17 -- INTERVAL 1 | 64 |

## SHIP STRUCTURE COMMITTEE

The SHIP STRUCTURE COMMITTEE is constituted to prosecute a research program to improve the hull structures of ships by an extension of knowledge pertaining to design, materials and methods of fabrication.

RADM W. M. Benkert, USCG (Chairman)
Chief, Office of Merchant Marine Safety
U.S. Coast Guard Headquarters

Mr. P. M. Palermo
Asst. for Structures
Naval Ship Engineering Center
Naval Ship Systems Command

Mr. John L. Foley
Vice President
American Bureau of Shipping

Mr. M. Pitkin
Asst. Administrator for
Commercial Development
Maritime Administration

Mr. C. J. Whitestone
Engineer Officer
Military Sealift Command

## SHIP STRUCTURE SUBCOMMITTEE

The SHIP STRUCTURE SUBCOMMITTEE acts for the Ship Structure Committee on technical matters by providing technical coordination for the determination of goals and objectives of the program, and by evaluating and interpreting the results in terms of ship structural design, construction and operation.

NAVAL SEA SYSTEMS COMMAND

Mr. R. Johnson - Member
Mr. J. B. O'Brien - Contract Administrator
Mr. C. Pohler - Member
Mr. G. Sorkin - Member

U.S. COAST GUARD

LCDR T. H. Robinson - Secretary
LCDR S. H. Davis - Member
CAPT C. B. Glass - Member
Dr. W. C. Dietz - Member

MARITIME ADMINISTRATION

Mr. F. Dashnaw - Member
Mr. N. Hammer - Member
Mr. R. K. Kiss - Member
Mr. F. Seibold - Member

MILITARY SEALIFT COMMAND

Mr. T. W. Chapman - Member
CDR J. L. Simmons - Member
Mr. A. B. Stavovy - Member
Mr. D. Stein - Member

AMERICAN BUREAU OF SHIPPING

Mr. S. G. Stiansen - Chairman
Dr. H. Y. Jan - Member
Mr. I. L. Stern - Member

NATIONAL ACADEMY OF SCIENCES
SHIP RESEARCH COMMITTEE

Mr. O. H. Oakley - Liaison
Mr. R. W. Rumke - Liaison

SOCIETY OF NAVAL ARCHITECTS &
MARINE ENGINEERS

Mr. A. B. Stavovy - Liaison

WELDING RESEARCH COUNCIL

Mr. K. H. Koopman - Liaison

INTERNATIONAL SHIP STRUCTURES
CONGRESS

Prof. J. H. Evans - Liaison

U.S. COAST GUARD ACADEMY

CAPT W. C. Nolan - Liaison

STATE UNIV. OF N.Y. MARITIME COLLEGE

Dr. W. R. Porter - Liaison

AMERICAN IRON & STEEL INSTITUTE

Mr. R. H. Sterne - Liaison

U.S. NAVAL ACADEMY

Dr. R. Bhattacharyya - Liaison

U.S. MERCHANT MARINE ACADEMY

Dr. Chin-Bea Kim - Liaison

## INTRODUCTION

In the analysis of the wave-induced ship hull strain data obtained by SSC in the 1960's it was necessary to infer the wave environment from estimated Beaufort wind speeds. An extraordinary amount of work was required to develop the inferential techniques. These techniques appear to suffice for valid prediction of long-term trends because a great deal of averaging is carried out. Unfortunately when verification of short-term statistical predictions is desired, the use of wind as a wave environment index appears to be less than satisfactory.

As a consequence it was one of the objectives of the SL-7 full-scale instrumentation program to provide a direct instrumental measure of the wave environment so that more precise correlations could be made between full-scale observations, and analytical and model results.

To this end the ship was fitted with a micro-wave radar relative wave meter and various motion sensing devices. A "Tucker Meter" pressure actuated wave height sensing system was also installed.

The purpose of the present project is to reduce and analyze the resulting wave meter data obtained on the SEA-LAND McLEAN in the second (1973-1974) and third (1974-1975) winter recording seasons.

The purpose of the present report is to document the various analyses carried out so as to produce the basic data reduction system, and to describe that system.

## BACKGROUND

In the documentation of the present project it has been necessary for practical reasons to assume on the part of the reader a general familiarity with the Ship Structure Committee's SL-7 measurement program. The primary background references for the present project are References 1 through 4. Reference 1 is the basic documentation of the full-scale instrumentation system. References 2 and 3 contain, for both recording seasons in question, a quite full account of instrumentation, basic recording, and the nominal circumstances surrounding the present data. These references also contain results of analyses of longitudinal vertical midship bending stress which were carried out according to the methods of Reference 4.

The first report under the present project is Reference 5. This reference contains the detail of the selection of the data set for the 1973-1974 winter season, the methods utilized in the digitization, the calibration of the data, and results of a first analysis of the data.

## PRELIMINARY DISCUSSION

### Overall Limitations and Goals

The present state-of-art of prediction or extrapolation of ship motions or stresses is grounded firmly in the linear short-term random approach as first put together by St. Denis and Pierson (References 6,7). Under this model the seaway is characterized by a directional variance spectrum, and is assumed to be statistically stationary and Gaussian. Because the ship responses are assumed to be linear functions of the seaway, they are also stationary and Gaussian, and may be characterized by variance spectra.

As a practical matter, the ultimate results of any full-scale instrumentation program are interpreted in light of the linear random model. In the data reduction of ship responses the absolute minimum requirement is to produce the statistical variance, or its square root (rms), or a theoretically related statistic such as the average or root-mean-square deviation of the maxima of a record from zero. When simple time histories are involved as raw material, the data reduction cake is often usefully iced with various statistics of the maxima and minima of the record (the extremes, the average of 10th highest, etc.). Finally, for some correlation purposes, estimates of the variance spectra may be desired and can be obtained with standard techniques.

In general, when the measurement of sea waves from a moving ship is considered, some considerable complication enters the data reduction picture. The complication arises from two sources:

a. Short crestedness of the seaway.
b. Speed of advance of the ship.

In the case of the wave measuring instrumentation installed in the SEA-LAND McLEAN, the best that can be expected is that the reduced data will represent the wave elevations at a point moving with the ship. Thus, even at best, the two complications just mentioned are of concern in the present problem.

According to the basic model, the directional spectrum of encounter is equal to the directional wave spectrum times a frequency mapping. The frequency mapping simply converts the point of reference from a fixed point (wave frequency) to a moving point (encounter frequency). Because the waves do not change with arbitrary changes in coordinate systems, the frequency mapping preserves variance. According to the assumptions in the basic model, the integration of the directional spectrum over direction and frequency is the variance. Furthermore, an adequate estimate of the variance may be obtained with knowledge of the time variation of wave elevation at a single point. Accordingly, there is no basic theoretical obstacle to the estimation of the seaway variance from elevations at a moving point.

Within the frame of reference of the basic statistical model the same arguments hold for averages of maxima of wave elevation time histories, with the interpretative exception that the resulting estimates of wave elevations (or heights) must be considered to be indicative only of the rise and fall along the track of the ship -- no information about short or long crestedness is involved and no information about wave directionality.

Thus the time history of wave elevation at a moving point can theoretically yield reasonable estimates of wave variance or average maxima. There are some circumstances where this is not practically so. Consider the situation in following or quartering seas where the predominant wave energy is concentrated in a narrow frequency and directional band and the typical component of wave celerity in the direction of ship advance is equal to ship speed (a 500-ft, 10-sec following wave for 30-kt ship speed, for instance). In this circumstance, the apparent wave elevation at the moving point will be slowly varying or practically constant for a short sample, and the typical variance estimate (which involves correction to zero sample mean) can be appreciably in error. This is a sampling problem rather than theoretical, but is nonetheless real and must be considered. There will undoubtedly be some "loss" in variance in following sea samples regardless of the distribution of variance in the actual directional wave spectrum.

There is a much higher order of complication in the spectrum of wave elevations at a moving point. Supposing a true time history to be available from a wavemeter -- the spectrum of this function of time takes the following form:

$$U(\omega_e) = \int S_1(\omega_e, X_e)\, dX_e + \int S_2(\omega_e, X_e)\, dX_e + \int S_3(\omega_e, X_e)\, dX_e \qquad (1)$$

where

$U(\omega_e)$ = spectrum of encounter at a moving point

$S_i(\omega_e, X_e)$ = directional spectrum of encounter, mapping region i

$\omega_e$ = encounter frequency

$X_e$ = wave-ship heading

To map the actual directional wave spectrum into the encounter plane, it must be divided into three regions of $\omega$ and $X$ where unique one-to-one mappings exist. In general, there may be a contribution to the spectrum at a given encounter frequency from three different wave frequencies. As shown, the directional spectrum is imbedded in an integral equation. Even if only one region is involved in the actual directional spectrum (a fairly narrow directional spread in head seas for instance) there will be insufficient data contained in the time history of one of

the wavemeters under discussion to derive any directional properties. The scalar wave spectrum (integration over heading) is derivable if the ship speed is zero. In summary, the directional wave spectrum is a function of time and space (frequency and direction). Multiple wavemeters are required at zero ship speed to provide even the possibility of obtaining directional spread. The scalar wave spectrum is not, in general, derivable with only one piece of data if the ship is at speed.

Clearly, it will not be possible to extract everything that could be desired from the present wavemeter data -- a limitation which was accepted at the very outset of the program. However, the overall full-scale/theoretical/model correlation problem is such that instrumental measurement of even the simplest wave statistic represents a potentially significant improvement, and thus the extraction from the data of these simple statistics is the basic minimum goal of the present project.

## ANALYSIS OF THE RADAR WAVE HEIGHT SYSTEM

### General Analysis

The characteristics of the radar system (the "OWHS Radar") are detailed in Reference 8. Essentially, the radar yields the range from the radar dish to the water surface. Because the radar is aimed at an angle with respect to ship co-ordinates, the radar output is called the "slant range." The radar system carried out only one further step in processing, and that is to subtract a nominal "initial" range from the instantaneous range before carrying out a digital to analog conversion. The initial nominal range upon ship's departure was not recorded. This was apparently because the system has automatic features which insure automatic acquisition of the initial range -- and re-acquisition in case of temporary return signal loss.

Thus the radar yields only a <u>measure</u> of the <u>relative</u> motion between ship and wave. The main effort in the present radar data reduction process is to correct this relative range for angular and vertical motion of the ship, and in so doing arrive at an estimate of the encountered wave elevations.

Conceptually, the correction of the radar range for ship angular orientation is a straight-forward vector operation. Unfortunately, the nature of the radar system makes it impossible to establish the length of the range vector solely from the instrumental data. The only reasonable option appeared to be to assume that: a) the sample mean of the radar data in each interval corresponds to the position of the nominal still water, zero speed, waterline of the ship; b) to correct the instrumental data to this mean; and c) to add to the corrected data the distance from radar antenna to still water as computed from the ship's departure drafts. If the sample mean is really reasonably close to the still water waterline this procedure might result in total range errors of 2 → 4 feet out of 75. Since the corrections are of a cosine nature it is thought

that the final results will not be too far off the mark. Unfortunately, however, it is not possible to find out just how far wrong the above procedure might be in any given case.

As noted in Reference 5, the signal re-acquisition feature also apparently produced large sudden shifts in the mean value of the radar signal. It was thought best to try to eliminate instances of this behavior from the data set rather than attempt analysis.

To simplify the analysis it was assumed that the range had been corrected for the initial bias as noted above. The situation may then be outlined in a general way as in Figure 1, in which the static (in harbor) case is to the left and the dynamic case is shown to the right.

There are three types of hardware in the system, all fixed in the ship.

1. The radar
2. An accelerometer package
3. Angular motions transducers.

The accelerometer package is intended to yield the vertical translation of the ship at that point. It is thus helpful to establish a fixed vertical reference plane parallel to the mean water surface (normal to local gravity) which passes through the accelerometer package when the ship is at rest in calm water. This situation is indicated at the left of Figure 1. The reference plane is (H-T) above mean water level, where:

H = Height of accelerometer package above baseline
T = Local ship draft.

In the first four voyages in the second season the radar and the nearest accelerometers are not located at the same point on the ship. This fact is expressed in the left side of Figure 1 by the vector $\vec{Q}$ which is defined to be a fixed, three-dimensional position vector for the radar relative to the accelerometer package.

Note that it has been convenient to define positive vertical directions down. For this reason and for convenience in analysis the position of the radar package is shown above the radar though this is not generally so in the ship.

The radar is aimed in a three-dimensional sense and so the slant range for the static case is a constant position vector $\vec{S}$.

Adopting the notation:

$Q_z$ = vertical component of $\vec{Q}$
(positive directed downward)

$S_z$ = vertical component of $\vec{S}$
(positive directed downward)

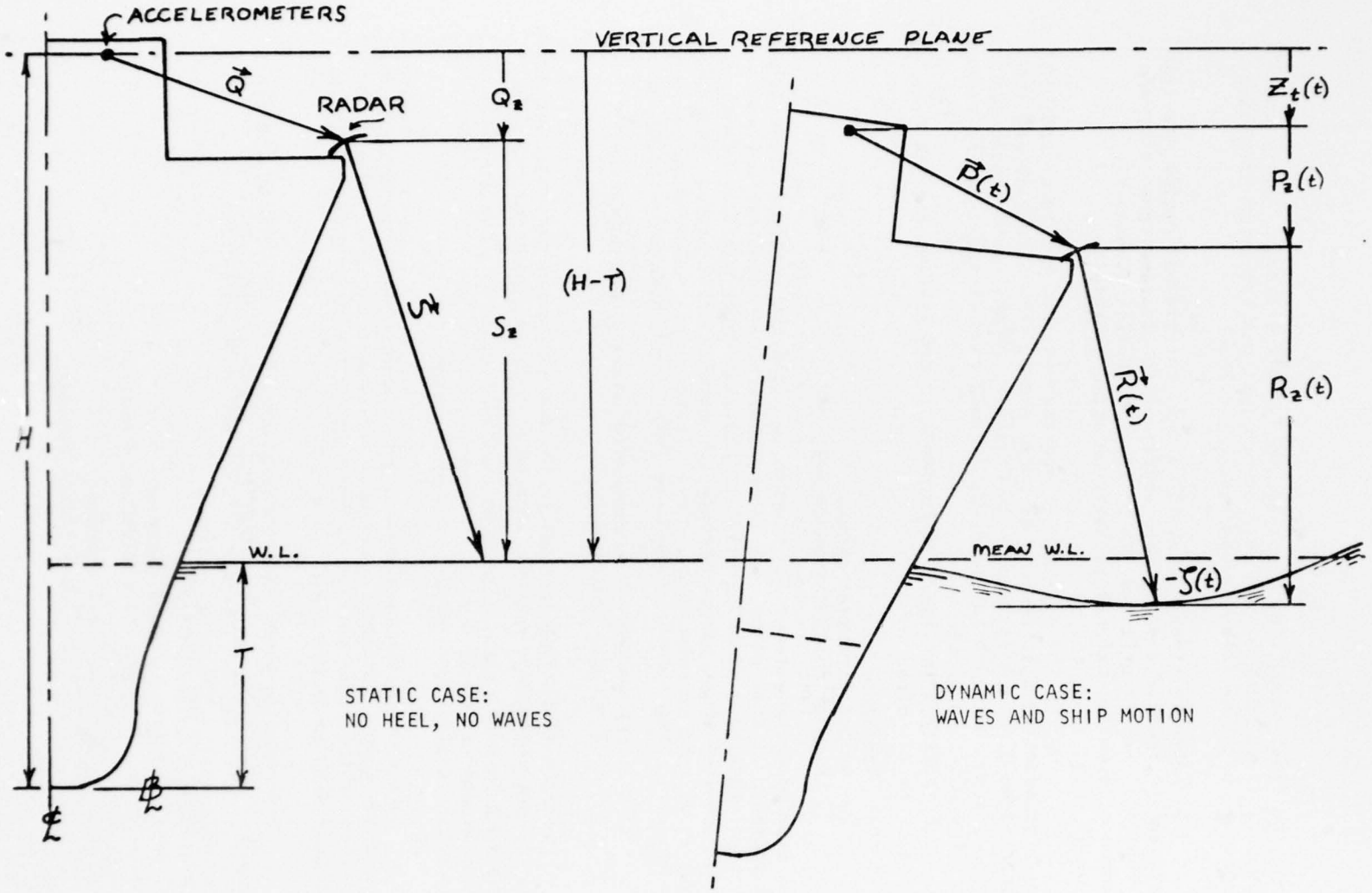


FIGURE 1 OVERALL GEOMETRY - RADAR

Thus:

$$(H-T) = Q_z + S_z \qquad (2)$$

(by definition)

Now proceeding to the dynamic case (right side of Fig.1), the ship is assumed to translate and rotate. The reference planes are as before, but the local water surface deviates from mean. The wave elevation, a function of time, is defined as $\zeta(t)$, positive upward (to correspond to the usual ideas about the ups and downs of waves).

The quantity $Z_t(t)$ is the vertical translation of the accelerometer package.

The position of the radar relative to the accelerometer is expressed by the vector $\vec{P}(t)$. This vector is the same as $\vec{Q}$ relative to the ship, but is in a different direction relative to fixed co-ordinates due to angular motion of the ship.

Finally the slant range is defined to be $\vec{R}(t)$. Relative to ship co-ordinates the slant range has the same direction as $\vec{S}$. Relative to fixed coordinates the direction is different according to the ship's angular motion.

The vertical components of the vectors are:

$P_z(t)$ = vertical component of position vector -- positive down.

$R_z(t)$ = vertical component of slant range vector -- positive down.

The component $P_z(t)$ is a function of time through the time variation of pitch and roll. The component $R_z(t)$ is a function of time for the same reasons -- in addition to the variation of $|\vec{R}(t)|$, which is the quantity measured.

All of the parts of the problem have now been indicated in a general way. From Figure 1 the general expression for the wave elevation may be written:

$$-\zeta(t) = Z_t(t) + P_z(t) + R_z(t) - Q_z - S_z \qquad (3)$$

Equation (3) is the basic framework for the data reduction process. Because the geometry is three-dimensional the expressions are deceptively simple with respect to implementation. The additional analysis required may be divided into several problem areas of which the first few appear as follows:

1. Provision of consistent axis systems and the required transformations between ship and fixed co-ordinates.

2. Expansion of vectors $\vec{P}(t)$ and $\vec{R}(t)$ into forms compatible with the data, and computation of $P_z(t)$ and $R_z(t)$

3. Analyses of angle transducers.

4. Consideration of the generation of the vertical component of acceleration and its double integration.

Axis System

To start, an axis system fixed in the ship and one fixed in space may be adopted in accordance with the Eulerian conventions in common use, Reference 9. It is supposed that a right handed set of axes is fixed relative to the earth o that the $X_o$, $Y_o$ axes are horizontal and the $Z_o$ axis is directed downward. The set of axes fixed in the ship (x,y,z) are so chosen that it is initially coincident with the fixed axes.

The x axis is positive forward, the y axis is positive to starboard, and the z axis is positive downward.

In order to express the position of a point in the ship in terms of the fixed co-ordinate system define:

$$\begin{aligned} X_t &= (X_o) \text{ co-ordinate of position of origin of ship axes} \\ Y_t &= (Y_o) \text{ co-ordinate of position of origin of ship axes} \\ Z_t &= (Z_o) \text{ co-ordinate of position of origin of ship axes} \end{aligned} \tag{4}$$

and $(x_1, y_1, z_1)$ = co-ordinates of the point with respect to the ship axes

Then the co-ordinates of the point in terms of the fixed axis system are:

$$\begin{aligned} X_1 &= X_t + a_{11}x_1 + a_{12}y_1 + a_{13}z_1 \\ Y_1 &= Y_t + a_{21}x_1 + a_{22}y_1 + a_{23}z_1 \\ Z_1 &= Z_t + a_{31}x_1 + a_{32}y_1 + a_{33}z_1 \end{aligned} \tag{5}$$

where the $a_{ij}$ are the direction cosines between the ship axes and the fixed axes.

Following the cited conventions, the direction cosines are derived from three operations:

1. Rotate the $X_o$, $Y_o$ axes about $Z_o$ an angle of yaw $\psi$.
2. Rotate the result about the body axis y through an angle of pitch, $\theta$.
3. Rotate this result about the body axis x through the angle of roll, $\varphi$.

The right hand rule is followed so that yaw is positive as the bow moves starboard, pitch is positive as bow moves up, and roll is positive starboard side down. The direction cosines resulting from these conventions are:

DIRECTION COSINES ($a_{ij}$) OF BODY AXES RELATIVE TO FIXED AXES IN TERMS of $\theta$, $\varphi$, $\psi$.

| | j=1 | j=2 | j=3 |
|---|---|---|---|
| i=1 | $\cos\theta \cos\psi$ | $-\cos\varphi \sin\psi + \sin\theta \sin\varphi \cos\psi$ | $\sin\varphi \sin\psi + \sin\theta \cos\varphi \cos\psi$ |
| i=2 | $\cos\theta \sin\psi$ | $\cos\varphi \cos\psi + \sin\theta \sin\varphi \sin\psi$ | $-\sin\varphi \cos\psi + \sin\theta \cos\varphi \sin\psi$ |
| i=3 | $-\sin\theta$ | $\cos\theta \sin\varphi$ | $\cos\theta \cos\varphi$ |

Now in the present problem the interest is in the vertical components of motion, and in any event there is not enough data being acquired to make yaw a useful input. Accordingly, the earth-fixed co-ordinate system $X_o$, $Y_o$, $Z_o$ is of little direct use in the problem and a semi-fixed coordinate system to provide vertical reference is more to the point. If the ship is assumed always to travel in the direction of positive $X_o$ and the translation $X_t$ of Eq. (4) is assumed to be ship velocity times time, the relations between the new semi-fixed axis system and the ship axes are found by substituting $X_t = 0$ and $\psi = 0$ in Eq. (5) and in the above table of direction cosines.

Defining co-ordinates of a point in the semi-fixed system as X, Y, Z the result for a point (x,y,z) in the ship system becomes:

$$\begin{aligned} X &= b_{11}x + b_{12}y + b_{13}z \\ Y &= Y_t + b_{21}x + b_{22}y + b_{23}z \\ Z &= Z_t + b_{31}x + b_{32}y + b_{33}z \end{aligned} \qquad (6)$$

and the direction cosines $b_{ij}$ are as follows:

DIRECTION COSINES ($b_{ij}$) OF BODY AXES RELATIVE TO SEMI-FIXED AXES IN TERMS OF $\theta$, $\varphi$

| | j=1 | j=2 | j=3 |
|---|---|---|---|
| i=1 | $\cos\theta$ | $\sin\theta \sin\varphi$ | $\sin\theta \cos\varphi$ |
| i=2 | 0 | $\cos\varphi$ | $-\sin\varphi$ |
| i=3 | $-\sin\theta$ | $\cos\theta \sin\varphi$ | $\cos\theta \cos\varphi$ |

Figure 2 indicates the sign conventions and the order of introducing angular motion (pitch-roll) for zero translation of the ship axis system.

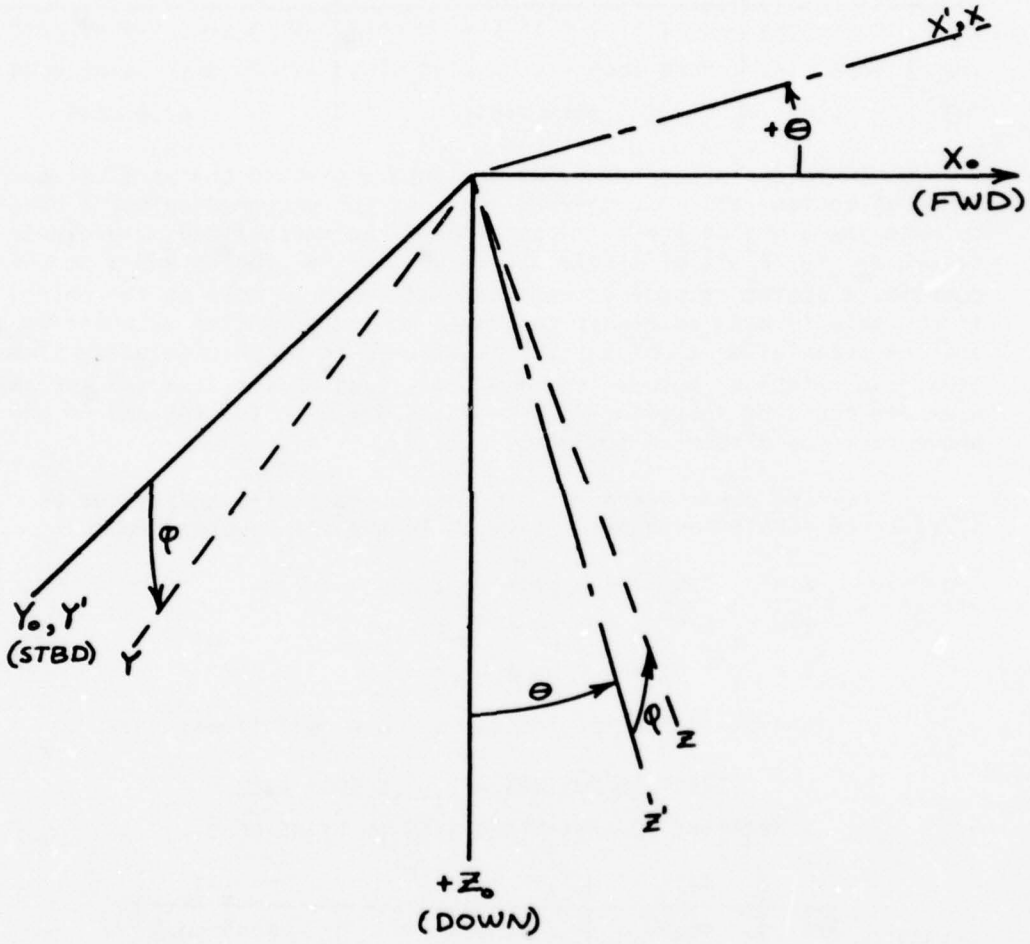


FIGURE 2 SEMI-FIXED AND MOVING AXIS SYSTEMS
(NO HEAVE OR SWAY)

Expansion of the Slant Range Vector

The orientation of the radar antenna is specified by an azimuth relative to the bow and a depression angle from the horizontal.

Referring to Figure 3, the azimuth angle ($\gamma$) is defined as positive for a swing to starboard. The depression angle ($\delta$) will be considered positive in the direction of the z axis. Defining direction cosines of the vector $\vec{S}$ (and $\vec{R}$ relative to ship coordinates) with respect to ship co-ordinates x,y,z as $c_1$, $c_2$, $c_3$:

Then
$$c_1 = \cos\gamma \cos\delta$$
$$c_2 = \sin\gamma \cos\delta$$
$$c_3 = \sin\delta \tag{7}$$

which is to say:

$$S_x = |\vec{S}|\, c_1 = |\vec{S}| \cos\gamma \cos\delta$$
$$S_y = |\vec{S}|\, c_2 = |\vec{S}| \sin\gamma \cos\delta$$
$$S_z = |\vec{S}|\, c_3 = |\vec{S}| \sin\delta \tag{8}$$

Now defining:

$$S_o = |\vec{S}|$$
$$R_a(t) = |\vec{R}(t)| \tag{9}$$

($S_o$ and $R_a(t)$ correspond to the absolute range from the radar)

Following Eq. (6) and considering only the relations between the antenna and the end of the ranges:

$$S_z = S_o\, c_3 \tag{10}$$

$$R_z(t) = R_a(t)\left\{-c_1 \sin\theta + c_2 \cos\theta\sin\varphi + c_3 \cos\theta\cos\varphi\right\}$$
$$= R_a(t)[c_1 b_{31} + c_2 b_{32} + c_3 b_{33}] \tag{11}$$

Thus the absolute range of the radar is separated from the functions of ship roll and pitch.

Expansion of Radar Position Vector

It will be most convenient to specify the location of the radar relative to the accelerometer in terms of heights and offsets. Accordingly the components of the position vector $\vec{Q}$ are outlined in Figure 4. Specifically,

$Q_x$ = distance of radar forward of accelerometers. (positive forward)

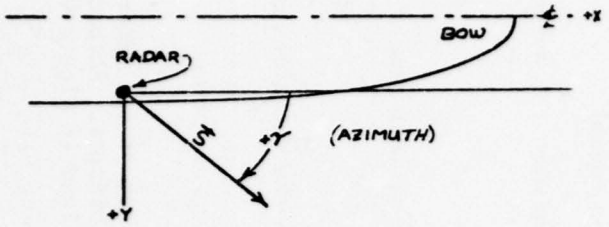


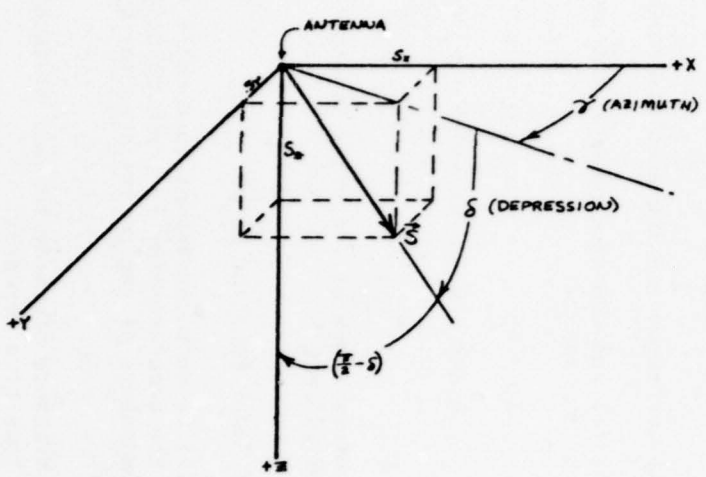


FIGURE 3 - RADAR AIMING NOTATION

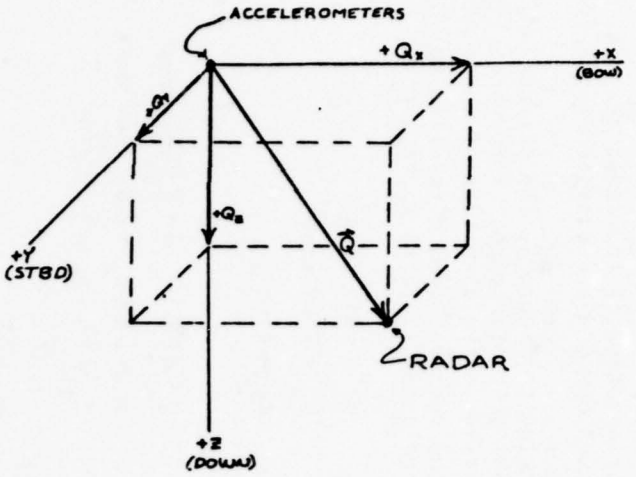


FIGURE 4 - RELATIVE POSITIONS OF ACCELEROMETERS AND RADAR

$Q_y$ = athwartship distance of radar from accelerometer. (positive to starboard)

$Q_z$ = vertical distance of radar below accelerometers -- positive for down (below), negative for radar above accelerometers.

Then from Eq. (6) as before:

$$P_z(t) = b_{31}Q_x + b_{32}Q_y + b_{33}Q_z$$

$$= -Q_x\sin\theta + Q_y\cos\theta\sin\varphi + Q_z\cos\theta\cos\varphi \qquad (12)$$

The Vertical Component of Acceleration

The accelerometer packages installed in the ship are bi-axial (vertical-athwartship) and each accelerometer is of the seismic type.

Seismic accelerometers are sensitive to angular orientation of their sensitive axis in that a signal component due to gravitational attraction is produced which is generally indistinguishable from true acceleration. In particular, the apparent acceleration (in g's) due to gravity is equal to the cosine of the angle between the accelerometer's sensitive axis and true vertical.

For analysis purposes a tri-axial accelerometer package will be assumed. The sensitive axes of the accelerometers are assumed aligned parallel to the ship fixed (x,y,z) axes (Fig.2). The signals from the three accelerometers are defined:

$A_x(t)$ = output from accelerometer aligned with x-axis

$A_y(t)$ = output from accelerometer aligned with y-axis

$A_z(t)$ = output from accelerometer aligned with z-axis

Positive acceleration will be defined as being in the positive direction of the x,y,z axes and the dimensions of all outputs are assumed to be in g's.

It is conventional to electronically offset the output of a vertically oriented accelerometer to compensate for constant gravity -- that is to consider the output as zero when the ship has no heel and is at rest in calm water. Accordingly, for present purposes the apparent acceleration signal from the accelerometer on the z axis will be

$$(A_z(t) - 1)$$

The cosines of the angles between the sensitive axes of the accelerometers and the $Z_o$ axis (vertical) are given in the table following Eq. (6). Thus the component of the sensed accelerations due to gravity are (in g's):

along x axis: $-b_{31} = +\sin\theta$

y axis: $-b_{32} = -\cos\theta\sin\varphi$

z axis: $-b_{33} = -\cos\theta\cos\varphi$

(Note that the negative sign is because deflection of accelerometer mass is opposite to that defined as positive acceleration.) Thus the sensed accelerations corrected for the influence of gravity are:

x axis -- $A_x(t) + b_{31}$

y axis -- $A_y(t) + b_{32}$

z axis -- $A_z(t) - 1 + b_{33}$

When there is no dynamic component and no list or trim, the total z-component = -1 = gravity component; = $-b_{33}$; and $A_z(t) = 0$. The above three components define a corrected translational acceleration vector defined in ship co-ordinates. For purposes of double integration, the component along true vertical is required and this is obtained by exercising Eq. (6):

$$A_v(t) = b_{31}A_x(t) + b_{32}A_y(t) + b_{33}A_z(t) - (b_{33}-1) \qquad (13)$$

In the present instrumentation setup there are no x-axis accelerometers. What is assumed is that the mass of the ship is so large relative to longitudinal excitation forces that the true longitudinal acceleration is zero. Exercising Eq. (6) and simplifying, the true longitudinal acceleration (component on x axis) becomes:

$$A_L(t) = b_{11}A_x(t) + b_{12}A_y(t) + b_{13}A_z(t) - b_{13} \qquad (14)$$

Assuming $A_L(t) = 0$ and manipulating Eq. (14) an estimate for the unmeasured component becomes:

$$A_x(t) = -\frac{b_{12}}{b_{11}}A_y(t) - \frac{b_{13}}{b_{11}}(A_z(t) - 1) \qquad (15)$$

Substituting in Eq. (13) there results the following estimate of true vertical acceleration:

$$A_v(t) = A_y(t)\left\{b_{32} - \frac{b_{12}}{b_{11}}b_{31}\right\} + A_z(t)\left\{b_{33} - \frac{b_{13}}{b_{11}}b_{31}\right\} + 1 - b_{33} + \frac{b_{13}}{b_{11}}b_{31}$$

and upon substitution of the expressions for $b_{ij}$ and some reduction:

$$A_v(t) = \frac{\sin\varphi}{\cos\theta}A_y(t) + \frac{\cos\varphi}{\cos\theta}A_z(t) - \left[\frac{\cos\varphi}{\cos\theta} - 1\right] \qquad (16)$$

Equation (16) is then the final result for the vertical acceleration under the assumption that no true longitudinal acceleration is present.

Regardless of the assumption about true longitudinal acceleration the true transverse acceleration ($A_T(t)$) turns out to be:

$$A_T(t) = \cos\varphi A_y(t) - \sin\varphi(A_z(t)-1) \tag{17}$$

Relationship Between Ideal Pendulum Transducer Outputs and Euler Angles

In the present case the pitch and roll transducers are of the pendulum type and are fixed in the ship. In each, the pendulum is constrained to move in a plane normal to its axis. For pitch the plane of motion is the x-z plane, (rotation about y axis) and for roll, rotation about the x axis in the y-z plane. If the pendulum transducer is working ideally (or statically) the pendulum aligns itself with the intersection of its plane of freedom and the plane in which lie both its rotation axis and the semi-fixed vertical, $Z_o$.

Referring to Figure 2, and assuming the roll pendulum, the pendulum is free to rotate in the y-z plane about the x axis and is in equilibrium along the intersection of this plane with the x-$Z_o$ plane. This intersection is noted z' in Figure 2 by virtue of the convention about pitching the ship first. The direction cosines of this line with respect to the fixed $X_o$, $Y_o$, $Z_o$ axes are

$$(\sin\theta,\ 0,\ \cos\theta)$$

The angle indicated by the pendulum is that between z and z' in Figure 2 since in the zero or up-right position of the ship $\varphi = 0$ and z and z' are coincident. The direction cosines of z are:

$$(\sin\theta\cos\varphi,\ -\sin\varphi,\ \cos\theta\cos\varphi)$$

Accordingly the cosine of the angle sensed by the pendulum is:

$$\sin^2\theta\cos\varphi + \cos^2\theta\cos\varphi = \cos\varphi$$

and the ideal roll pendulum output is the same as $\varphi$ in the previous section, and the sign convention will be assumed to be the same.

Now considering pitch, the plane of rotation of the pendulum is defined by y=0. The direction cosines of the normal to the plane (the y axis) are:

$$(\sin\theta\sin\varphi,\ \cos\varphi,\ \cos\theta\sin\varphi)$$

Accordingly, the direction cosines of the pendulum ($\ell$,m,n) at any position in its plane of rotation must satisfy:

$$0 = \ell\ \sin\theta\sin\varphi + m\ \cos\varphi + n\ \cos\theta\sin\varphi$$

At equilibrium the pitch pendulum must also lie in the y-$Z_o$ plane. This plane is not coincident with the $Y_o$-$Z_o$ plane because of the roll angle and thus the ideal pitch pendulum output is not the same as the Euler pitch angle $\theta$.

Assume the direction cosines of the normal to the y-$Z_o$ plane are $(p,q,r)$. The normal to the plane must also be normal to the $Z_o$ axis which results in r=0. The normal to the plane is also normal to the y axis and this requirement means:

$$0 = p\sin\theta\sin\varphi + q\cos\varphi + r\cos\theta\sin\varphi$$

Finally the direction cosines must satisfy the relationship

$$p^2 + q^2 + r^2 = 1$$

With these relations the direction cosines of the normal to the y-$Z_o$ plane become:

$$p = 1/\sqrt{1 + \sin^2\theta\tan^2\varphi}$$

$$q = -\sin\theta\tan\varphi/\sqrt{1 + \sin^2\theta\tan^2\varphi}$$

$$r = 0$$

From this result it follows that the direction cosines of the equilibrium position of the pendulum $(\ell,m,n)$ must satisfy

$$0 = \ell - m\sin\theta\tan\varphi$$

They must also satisfy

$$\ell^2 + m^2 + n^2 = 1$$

as well as the equation derived previously for the x-z plane:

$$0 = \ell\sin\theta\sin\varphi + m\cos\varphi + n\cos\theta\sin\varphi$$

Solution of the three relations simultaneously yields

$$\ell = \frac{-\sin\theta\cos\theta\tan\varphi\sin\varphi}{\pm\sqrt{1+\sin^2\theta\tan^2\varphi}}$$

$$m = \frac{-\cos\theta\sin\varphi}{\pm\sqrt{1+\sin^2\theta\tan^2\varphi}}$$

$$n = \cos\varphi\sqrt{1+\sin^2\theta\tan^2\varphi}$$

The angle sensed by the pitch pendulum will be called $(\alpha)$ and it is the angle between the equilibrium position defined above and the z axis. Accordingly,

$$\cos\alpha = \ell b_{13} + m b_{23} + n b_{33}$$

$$= \cos\theta/\sqrt{1+\sin^2\theta\tan^2\varphi} \qquad (18)$$

Manipulating Eq. (18), there results the relations between the observed angle $\alpha$ and the required angle $\theta$ (for $|\varphi| < \pi/2$):

$$\cos\theta = \frac{\cos\alpha}{\cos\varphi\sqrt{(1+\cos^2\alpha\tan^2\varphi)}}$$

$$\sin\theta = \frac{\sin\alpha}{\pm\sqrt{1+\cos^2\alpha\tan^2\varphi}} \tag{19}$$

Clearly for zero or very small roll $\alpha$ and $\theta$ are nearly the same, which is according to reason.

The preceding development allows the functions of the Euler angles to be expressed in terms of the ideal observable angles.

It is assumed that the sense of the pendulum output is the same as noted in Figure 2:

$\varphi$ = Roll angle as observed by pendulum transducer -- positive for starboard side down.

$\alpha$ = Pitch angle as observed by pendulum transducer -- positive for ship bow up.

The functions required by the development in previous sections are:

$$b_{31} = -\sin\theta = \frac{-\sin\alpha}{\pm\sqrt{1+\cos^2\alpha\tan^2\varphi}} \tag{20}$$

$$b_{32} = \cos\theta\sin\varphi = \frac{\cos\alpha\tan\varphi}{\pm\sqrt{1+\cos^2\alpha\tan^2\varphi}} \tag{21}$$

$$b_{33} = \cos\theta\cos\varphi = \frac{\cos\alpha}{\pm\sqrt{1+\cos^2\alpha\tan^2\varphi}} \tag{22}$$

$$\left(\frac{\sin\varphi}{\cos\theta}\right) = \frac{\sin\varphi\cos\varphi}{\cos\alpha}\sqrt{1+\cos^2\alpha\tan^2\varphi} \tag{23}$$

$$\left(\frac{\cos\varphi}{\cos\theta}\right) = \frac{\cos^2\varphi}{\cos\alpha}\sqrt{1+\cos^2\alpha\tan^2\varphi} \tag{24}$$

Approximations to the Required Functions of Roll and Pitch Angles

Equations (20) through (24) are likely to be unnecessarily time consuming to evaluate and a reasonable simplification is desirable. The pitch and roll transducers have stops at $\pm 45^\circ$ so that neither angle sensed can be greater under any circumstances.

According to the typical results indicated in Reference 5, a "large" oscillatory pitch is $\pm$ 2 or 3 degrees and a "large" oscillatory roll is $\pm 15^\circ$. Considering natural limits, the magnitude of the largest pitch observed in model tests at D.L. (under unusually severe conditions) is $\pm 15^\circ$. In the present case a $10^\circ$ pitch moves the bow up (or down) about

90 feet or 3 times draft. Clearly, an approximation good to $\pm 10^{\circ}$ pitch seems more than adequate in the present case. Similar natural limits upon roll are not so obvious. Plus-or-minus $15^{\circ}$ is out of the usual small angle approximation range and was observed in the fourth voyage. Most seamen are willing to recount tales of $90^{\circ}$ out-to-out rolls ($\pm 45$ degrees). It appears conservative to split the difference, and so the objective as far as roll was concerned was to make an approximation good to $\pm 30^{\circ}$, and at least acceptable to $\pm 45^{\circ}$.

Toward this end the expressions in $\alpha$ and $\varphi$, Eqs. (20) through (24), were expanded in series retaining terms to 5th or 6th order. Finally, in each case the three or four terms of lowest order were retained. These approximations were compared with the exact evaluations of Eqs. (20) to (24) over a $\pm 10^{\circ}$ range of $\alpha$ and a $\pm 45^{\circ}$ range of $\varphi$. Some minor adjustment of coefficients was made to improve the correspondence with the exact evaluations for large angles and the final approximations are as follows:

$$b_{31} = \frac{-\sin\alpha}{\sqrt{1+\cos^2\alpha\tan^2\varphi}} \approx -\alpha + 0.1667\alpha^3 + 0.5\alpha\varphi^2 \qquad (25)$$

$$b_{32} = \frac{\cos\alpha\tan\varphi}{\sqrt{1+\cos^2\alpha\tan^2\varphi}} \approx \varphi - 0.1667\varphi^3 - 0.43\varphi\alpha^2 \qquad (26)$$

$$b_{33} = \frac{\cos\alpha}{\sqrt{1+\cos^2\alpha\tan^2\varphi}} \approx 1 - 0.49\varphi^2 - 0.5\alpha^2 + 0.7\,\alpha^2\varphi^2 \qquad (27)$$

$$\frac{\sin\varphi}{\cos\theta} = \frac{\sin\varphi\cos\varphi}{\cos\alpha}\sqrt{1+\cos^2\alpha\tan^2\varphi}$$

$$\approx \varphi - 0.1667\varphi^3 + 0.43\varphi\alpha^2 \qquad (28)$$

$$\frac{\cos\varphi}{\cos\theta} = \frac{\cos^2\varphi}{\cos\alpha}\sqrt{1+\cos^2\alpha\tan^2\varphi}$$

$$\approx 1 - 0.49\varphi^2 + 0.5\alpha^2 - 0.7\alpha^2\varphi^2 \qquad (29)$$

The range of the possible values of the coefficients in Eqs. (25) to (29) is in the interval $\pm 1$. The maximum absolute error in the approximations indicated is $\pm 0.001$ over the ranges $-10 \le \alpha \le 10^{\circ}$; $-30 \le \varphi \le 30^{\circ}$. The absolute error enlarges to $\pm .003$ to $\pm 0.006$ up to roll angles of $40^{\circ}$ and is $\pm .004$ to $\pm 0.013$ at $45^{\circ}$ roll.

The specified resolution of the radar is roughly 1 foot. If the approximations above are reasonable they should introduce errors much smaller than 1 foot for perfectly measured data. The magnitude of the range, $R_a(t)$, is in the neighborhood of 75 feet. If depression angles ($\delta$) between 60 and $70^{\circ}$ are chosen with azimuths ($\gamma$) between $45^{\circ}$ and $90^{\circ}$, the coefficients $c_1$, $c_2$, $c_3$, Eq. (7), vary roughly as follows:

$$0 < c_1 < .35$$
$$.24 < c_2 < .47$$
$$.87 < c_3 < .94$$

In the range: roll = $\pm 30^{\circ}$ and pitch = $\pm 10^{\circ}$ the magnitudes of $b_{31}$, $b_{32}$, $b_{33}$ are .16, .7 and 1. at most (with the worst combinations of signs), to that if <u>each</u> of the coefficients $b_{31}$, $b_{32}$, $b_{33}$ is in error by +0.001, the maximum error in the multiplier of $R_a(t)$ comes out to be about 0.0015 and this typically corresponds to an error of 0.1 feet. Errors in the approximations are not usually of the same sign so that the expected maximum error in the corrected range is significantly less than this. When roll angles are greater than $30^{\circ}$ the corresponding error is significantly greater, but the waves themselves would be expected to be large and the incluence of the approximation error relatively smaller.

Pretty much the same argument applies to the position component, $(P_z(t)-Q_z)$ Eq. (12). In this case the possible use of the midship accelerometer package is excluded because it has not been recorded on the same tape as the radar, roll and pitch. In any event it would be a poor choice since $Q_x$ would be $\approx$ 500 feet and an error of $1/2^{\circ}$ in $\theta$ would result in a 5 foot error in the position component. Of the two accelerometer packages remaining (Refs. 1,2,3) the one farthest from the radar has:

$$Q_x \approx 47 \text{ ft}$$
$$Q_y \approx 50 \text{ ft}$$
$$Q_z \approx -40 \text{ ft}$$

and:

$$P_z(t)-Q_z \approx 47\, b_{31} + 50\, b_{32} - 40\, (b_{33}-1)$$

The coefficient $(b_{33}-1)$ is always negative and at most is about -.15. The coefficients $b_{31}$ and $b_{32}$ are at most .16 and .7 so that for errors of +.001 in each coefficient the maximum error in $(P_z(t)-Q_z)$ due to the approximations appears to be about 0.05 feet. In the actual data reduction case the accelerometer package nearest the radar was used and thus the potential error is even less than that just cited.

Turning to the acceleration $A_v(t)$, Eq. (16), when roll is small the vertical accelerometer dominates, its coefficient is unity and the absolute .001 approximation error translates to 0.1%. When roll is large the horizontal acceleration has been observed to dominate and in this case the error might range between 0.2 and 0.5%.

It should be emphasized that all the above argument involves perfectly measured data. It appears that errors or possible lack of resolution in the basic range, acceleration and angle data may have a much greater influence upon error in the final product than the errors inherent in the approximations, Eqs. (25) to (29).

Error Analysis: Pendulum Transducers

The pendulum transducers are specified to have a 2 Hz or higher natural frequency with what appears to be between 0.4 and 0.7 times critical damping depending upon ambient temperature. Accordingly the errors due to the response of the instruments themselves should be negligible below 0.2 Hz and at least acceptably small below 0.4 Hz. It appeared from References 2 and 3 that little if any roll and pitch response occurs at frequencies greater than 0.3 Hz; that is, that the ship itself does not respond as a rigid body to excitations by waves which are short enough to result in encounter frequencies above 0.3 Hz. Because of the simplicity of the instrument, correction of data for the pendulum frequency characteristics would be feasible, but it appeared reasonable to ignore the pendulum dynamics altogether.

The above considerations do not remove all the potential dynamic problems from the pendulum transducers. For frequencies sufficiently below pendulum resonance the pendulum aligns itself along a line opposite to the direction of the resultant translational force on its pivot. If the pivot is not accelerating, this line is the local vertical. All the previous derivations of ideal pendulum angles have been for the static case or for the case of no translational acceleration of the pivot. The purpose of the present development is to assess the errors introduced by translations of the ship in way of the pendulum transducers.

First it will be assumed as in a previous development that the inertia of the ship is so large in relation to longitudinal excitation that fore and aft accelerations of the ship at the pendulum location are zero. It is known that the ship heaves and highly likely that it sways so that two translational accelerations may be assumed:

$A_T(t)$ = Horizontal acceleration in the direction of the (fixed) $Y_o$ axis, Figure 2. (in g's)

$A_V(t)$ = Vertical acceleration in the direction of the (fixed) $Z_o$ axis, Figure 2. (in g's)

(In the following the functional notation will be dropped and the time variation will be understood.)

With these assumptions and sense conventions, the $Y_o$ component of the translational force on the pendulum pivots is:

$(w\ A_T)$

the $X_o$ component is zero,

and the $Z_o$ component is:

$w\ (A_V - 1)$

(where w is the pendulum weight)

Thus the apparent gravity which the pendulum "sees" is a vector with:

$$X_o \text{ component} = 0$$
$$Y_o \text{ component} = -A_T$$
$$Z_o \text{ component} = 1-A_V$$

and which has direction cosines

$$p = 0$$
$$q = -A_T \Big/ \sqrt{A_T^2 + (1-A_V)^2}$$
$$r = (1-A_V) \Big/ \sqrt{A_T^2 + (1-A_V)^2}$$

As in the previous development the location of the pendulum is along the intersection of a plane perpendicular to its axis and a plane passing through the axis and the local gravity vector above. Once the direction cosines of the pendulum position $(\ell,m,n)$ are found the cosine of the angle the pendulum makes with the z axis can be found as in a previous section. This process was carried out for the pitch and roll pendulums and the results are as follows:

For the roll pendulum:

$$\cos\beta = \cos\varphi \frac{\cos\theta - \frac{q}{r}\tan\varphi}{\sqrt{\frac{q^2}{r^2} + \cos^2\theta}} \tag{30}$$

For the pitch pendulum:

$$\cos\tau = \frac{\cos\theta - \frac{q}{r}\tan\varphi}{\sqrt{1 + (\frac{q^2}{r^2} + \sin^2\theta)\tan^2\varphi - 2\frac{q}{r}\cos\theta\tan\varphi}} \tag{31}$$

where:

$\beta$ = the angle sensed by the roll pendulum
$\tau$ = the angle sensed by the pitch pendulum

Substitution of Eq. (29) and some purely algebraic manipulation serves to put Eqs. (30) and (31) in the following form:

$$\tan\beta = \frac{\tan\varphi + \bar{A}}{1 - \bar{A}\tan\varphi} \tag{32}$$

$$\tan\tau = \frac{\tan\alpha}{1 - \bar{A}\tan\varphi} \tag{33}$$

where

$$\bar{A} = \frac{q}{r}\,\frac{\cos\varphi\sqrt{1+\cos^2\alpha\tan^2\varphi}}{\cos\alpha} = \frac{q}{r\cos\theta} \tag{34}$$

Also following from Eqs. (32), (33):

$$\tan(\beta-\varphi) = \bar{A} \tag{35}$$

$$\tan(\tau-\alpha) = \frac{\bar{A}\tan\varphi\cos\alpha\sin\alpha}{1-\bar{A}\tan\varphi\cos^2\alpha} \tag{36}$$

These last two expressions are for the errors $(\tau-\alpha,\beta-\varphi)$ which are introduced by the translational accelerations of the pendulum. As written, the R.H. sides of Eqs. (32) to (36) involve only ideal parameters -- none of which can be observed directly by the installed instrumentation.

Ideally, there is the possibility of eliminating the unkown ideal parameters by using the outputs from the accelerometer package mounted alongside the pendulums. Equations for the true vertical and transverse accelerations are Eqs. (16) and (17). Combining these:

$$\frac{q}{r} = \frac{-A_T}{1-A_v} = \cos\theta\,\frac{A_y-(A_z-1)\tan\varphi}{(A_z-1)+A_y\tan\varphi} \tag{37}$$

and thus

$$\bar{A} = \frac{\bar{H}-\tan\varphi}{1+\bar{H}\tan\varphi}$$

$$\text{With:}\quad \bar{H} = \frac{A_y}{A_z-1} \tag{38}$$

Substitution of Eq. (38) into Eq. (32) yields:

$$\tan\beta = \bar{H} = \frac{A_y}{A_z-1} \tag{39}$$

No expression for the unknown angle, $\varphi$, results because both the accelerometers and the pendulum are seismic instruments. Both "see" the same effective local gravity vector and are both recording the same information. To correct sensed pendulum angles to true it is necessary to have an independent measure of the true transverse acceleration. To correct sensed accelerations to true vertical and transverse acceleration it is necessary to have an independent measure of <u>true</u> angles.

With the instrumentation installed there is no way to make the corrections to indicated angles which are implied by Eqs. (32) to (36).

As a practical matter the pitch errors shown in Eq. (36) are probably fairly small. Making the small angle approximation:

$$\frac{\tau-\alpha}{\alpha} \approx \bar{A}\varphi$$

A true transverse acceleration of the ship's C.G. of 0.1g might be quite a lot, and this coupled with $10^{o}$ roll yields errors of the order of 2%. If roll and sway are roughly in quadrature as expected, the error will be smaller. It should be remarked that the potential first order errors in pitch angle were <u>assumed</u> away at the outset by assuming $A_L(t) = 0$ (Eq.14).

The error situation with roll is not pleasant. A true transverse acceleration of 0.1g should correspond roughly to $5^{o}$ error, which could easily be relatively very large.

With the data at hand it must be assumed that actual sway accelerations are negligible in way of the pendulums -- there is no way to check this assumption with the data which has been acquired.

Recapitulation of Analysis Thus Far and Sample Evaluation

Substituting Eqs. (11) and (12) in Eq. (3), the expanded expression for the wave elevation becomes:

$$\begin{aligned} -\zeta(t) &= Z_t(t) + (P_z(t)-Q_z) + (R_z(t)-S_z) \\ &= Z_t(t) + b_{31}Q_x + b_{32}Q_y + (b_{33}-1)Q_z \\ &\quad + R_a(t)\left[c_1 b_{31} + c_2 b_{32} + c_3 b_{33}\right] - S_z \end{aligned} \tag{40}$$

The translation $Z_t(t)$ is the double integration of the true vertical acceleration at the accelerometer package location, Eq. (16):

$$\begin{aligned} A_v(t) &= \frac{d}{dt^2}\left[Z_t(t)\right] \\ &= \frac{\sin\varphi}{\cos\theta} A_y(t) + \frac{\cos\varphi}{\cos\theta} A_z(t) - \left[\frac{\cos\varphi}{\cos\theta} - 1\right] \end{aligned} \tag{41}$$

The notation is summarized for convenience as follows:

A. Parameters Fixed by Installation or Ship Geometry (Numerical values were noted in Ref. 5 for the second season).

$Q_x, Q_y, Q_z$ -- The coordinates of the radar position relative to the accelerometer position.

$S_z$ -- The vertical position of radar antenna above waterline.

$c_1, c_2, c_3$ -- Direction cosines of radar beam relative to ship-fixed co-ordinate system.

B. Recorded Functions of Time

$R_a(t)$ -- The indicated slant range, the actual range, not the variation of the range about some mean value.

$A_z(t), A_y(t)$ -- Vertical and horizontal acceleration signals as recorded by the fixed bi-axial accelerometer package.

$b_{ij}$ -- Functions of roll and pitch angles $\varphi$ and $\theta$; approximations, Eqs. (25) through (27).

The first four terms of Eq. (40) together are the variation in vertical position of the radar antenna from its nominal height above water, $S_z$. The $b_{ij}$ coefficients are complicated functions of time dependent angles. The slant range, $R_a(t)$, is the entire range -- not the deviations from some mean.

Because Eqs. (40) and (41) involve products of measured, time dependent, variables a great part of the implementation had to be in the time domain. In particular, there was no reasonable alternative to the computation of the quantities:

$$[-\zeta(t) - Z_t(t)] = R_c(t)$$

and; $A_v(t)$

in the time domain.

The "wave elevation" in Eq. (40) is not necessarily zero mean. The development thus far has been in terms of coordinates fixed for zero ship speed. When the ship is underway there will be small trims and heels constant for sample durations and probably some bodily sinkage. In addition there may also be some dynamic swell-up of water at the radar's point of aim. These things add up to a constant bias in the vertical position of the radar and a bias in the slant range itself. There is in addition the problem cited at the beginning of the analysis of the radar system; that is, the absolute value of the slant range cannot be known with great accuracy. The assumptions for coping with this were outlined previously, and make no provision for sinkage, dynamic swell-up, etc. Long term apparent biases cannot reasonably be handled in the integration for Z(t) because of the discontinuous nature of the records. However, a zero bias in the derived wave elevation is not serious since all the useful results from the final product involve an explicit or implicit correction to zero sample mean (spectra, variances, crest-to-trough heights, etc.). Accordingly, there was no particular point in attempting to specially consider biases, and it was decided to correct $R_c(t)$ and $A_v(t)$ to zero sample mean.

The programming of Eq. (4) and (41) is straightforward. The parameters necessary had been included in the calibrated data files described in Reference 5. The total radar slant range was approximated

according to the assumptions previously mentioned, and two new time histories were produced for each recording interval; $R_c(t)$ and $A_v(t)$. One particular interval was selected for the purpose of detailed numerical checking. This was run 401 which was the first interval on analog tape 145 (index 17). This particular run was chosen because the waves were high, all of the digitized signals were relatively large, and the ship was in head seas at low speed (8.7 knots).

Figures 5a and 5b are expanded time histories covering the first 300 odd seconds of this interval. Only the 5 data channels involved in this first phase of the data reduction are shown. At the top is the slant (raw) radar range corrected to zero sample mean (dashed line). Superimposed is the "corrected" range ($R_c(t)$), also corrected to zero sample mean. The next two frames down each page are scaled roll and pitch. Next in order are the "vertical" accelerations. The solid trace is $A_v(t)$, the "true vertical" acceleration. Superimposed in dashed lines is the observed body vertical acceleration, $A_z(t)$. Finally at the bottom is the observed body lateral acceleration, $A_y(t)$.

In the process of checking the numerical work and the relationships between the various channels it was found that the sense of pitch as stated in Reference 5 was opposite to what would be expected. At the relatively slow ship speed involved in this case the vertical acceleration forward should be nearer in-phase with pitch than out of phase. Also, the derived wave elevations (to be later displayed) implied that the bow was not lifting after passage of a wave crest. The strongest evidence that a sense was wrong was in the relationship between pitch and vertical acceleration. Because of the gravity bias in the vertical acceleration signal it was very difficult to believe that the sense of the acceleration was incorrect, and it was thus concluded that the pitch sense had to be reversed. This reversal was incorporated in the programming and in Figure 5. It thus should also be noted that the signs of the pitch extremes given in Reference 5 are reversed.

During this checking process, the relationship between the sample mean of pitch and electrical zero was reviewed. In many of the intervals digitized from the second season the sample mean differed from electrical zero (the stated zero pitch condition) by a much greater amount than would be expected in view of the fact that (for instance) a $1/2^{\circ}$ pitch bias corresponds to a 10 foot ship trim. Accordingly, it was felt best to correct both the angular responses to zero sample mean before processing.

An additional observation about pitch must be made. It may be noted that the pitch trace in Figure 5 is peculiarly asymmetrical. The large, sudden bow down (negative) pitches are most peculiar in view of the nominal wave conditions and ship speed. After completing the derivation of the wave trace corresponding to Figure 5, it was realized that the large time rates of change of bow down pitch to be occasionally seen apparently corresponded with the time the bow was plowing into particularly large individual waves. It is thus thought possible that the

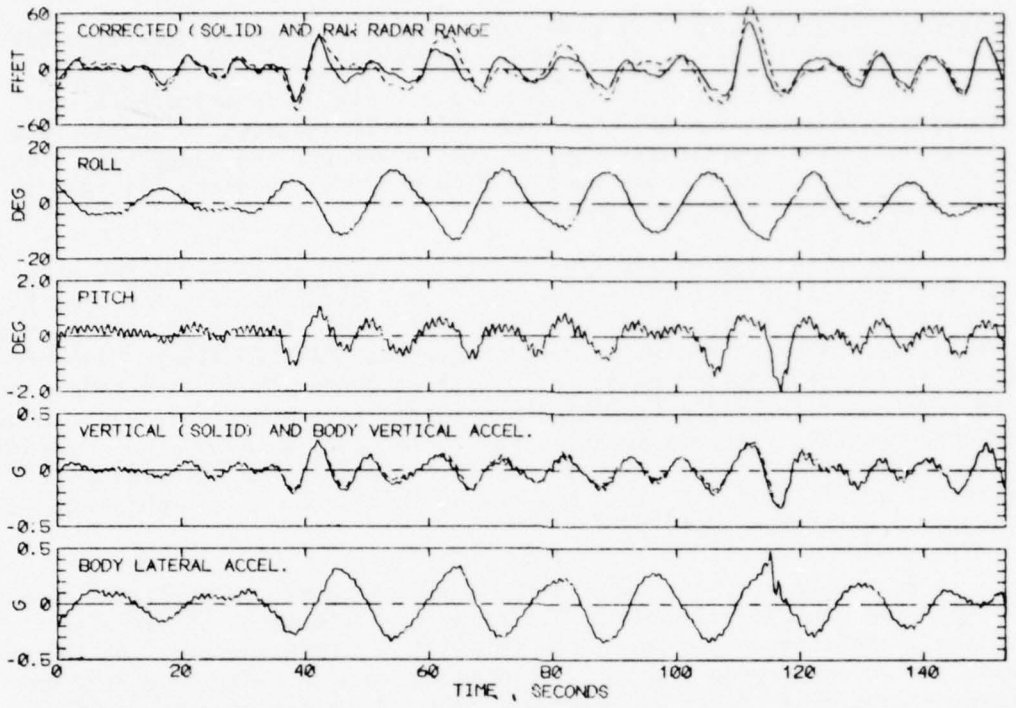


FIGURE 5a - SAMPLE TIME HISTORY, RUN 401

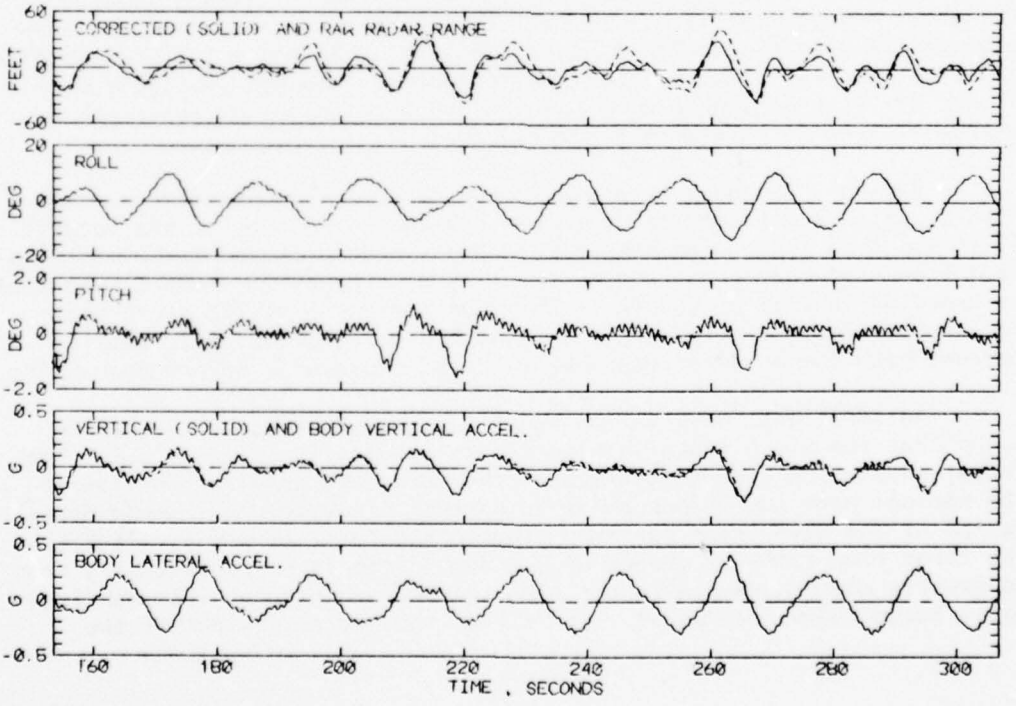


FIGURE 5b - SAMPLE TIME HISTORY, RUN 401

peculiar asymmetric negative pitch trace results from transient longitudinal deceleration of the ship. (A sudden longitudinal deceleration has the effect of moving the pendulum in an apparently bow down direction.) It is thus probable that the previously made zero longitudinal acceleration assumption is incorrect at times.

The object of this phase of the data reduction was to compute $R_c(t)$ and $A_v(t)$. It is obvious from Figure 5 that the difference between $A_v(t)$ and $A_z(t)$ is exceedingly small, despite the fact that the example involves some of the largest motions in the second season data set. Thus the problems about pitch just noted, and the previously noted question about the influence of sway upon the roll pendulum, appear not to be serious with respect to the accelerations.

Referring again to Figure 5, the differences between slant (raw) range and the "corrected" range, $R_c(t)$ are appreciable. Analysis of the detail of the numerical result revealed that the dominant terms in the correction are $b_{32}Q_y$, and $c_2 b_{32}$ in the multiplier of $R_a(t)$ in Equation (40). In Figure 5, $b_{32}Q_y$ is effectively the roll angle times half the ship beam. Thus for the cases where the accelerometer package was located in the radar pedestal the corrections should be much less. The reasons for the dominance of the terms involving $b_{32}$ are relatively simple. First, the actual aiming of the radar relative to the ship was at $90^o$ azimuth, $74^o$ depression -- almost vertical. This in conjunction with the cosine nature of the correction makes the vertical component of the slant range not as far different from the slant range as it could have been. (The correction is mostly just the cosine of the roll angle.) Secondly, the radar package in the case of Figure 5 is located nearly abeam of the radar. Thus both $b_{31}Q_x$ amd $(b_{33}-1)Q_z$ (Eq.40) are inherently small. The net indication from this is that the problem of the influence of sway on the roll pendulum is still a problem. Though the problem may mostly influence the answer for the voyages where the accelerometers were not in the radar pedestal, it was thought wise to plan on documenting roll in the final data reduction process.

Correction of Radar Range for Vertical Motion of the Ship

The purpose of the work is to produce time histories of wave elevation:

$$-\zeta(t) = R_c(t) + Z_t(t) \tag{42}$$

and/or the encountered spectrum of waves, $S_{\zeta\zeta}(\omega_e)$. Actually, both would be desirable results. There are two approaches possible to make an effective conversion of $A_v(t)$ to $Z_t(t)$ for purposes of Eq. (42).

The first approach involves manipulations of the acceleration and range spectra and cross-spectrum to result in a wave spectrum. In this approach no direct estimate of $-\zeta(t)$ is made. The method follows. The spectrum of wave elevation (Eq.42) may be written:

$$S_{\zeta\zeta}(\omega_e) = S_{RR}(\omega_e) + S_{ZZ}(\omega_e) + 2C_{RZ}(\omega_e) \tag{43}$$

where:

$S_{RR}(\omega_e)$ = spectrum of corrected range, $R_c(t)$
$S_{ZZ}(\omega_e)$ = spectrum of translation $Z_t(t)$
$C_{RZ}(\omega_e)$ = co-spectrum of $R_c(t)$ and $Z_t(t)$

Of the required terms, $S_{RR}(\omega_e)$ may be estimated since $R_c(t)$ is available from the previous data reduction phase. The other terms cannot be estimated directly. However the spectrum of $A_v(t)$ and the cross-spectrum of $R_c(t)$ and $A_v(t)$ may be estimated:

$S_{AA}(\omega_e)$ = spectrum of $A_v(t)$
$C_{RA}(\omega_e)$ = co-spectrum of $R_c(t)$ and $A_v(t)$

and the required spectra involving $Z(t)$ may then be estimated as:

$$S_{ZZ}(\omega_e) = \frac{1}{\omega_e^4} S_{AA}(\omega_e)$$

$$C_{RZ}(\omega_e) = \frac{-1}{\omega_e^2} C_{RA}(\omega_e)$$

so that:

$$S_{\zeta\zeta}(\omega_e) = S_{RR}(\omega_e) + \frac{1}{\omega_e^4} S_{AA}(\omega_e) - \frac{2}{\omega_e^2} C_{RA}(\omega_e) \tag{44}$$

So long as the estimated spectra derived from accelerations approach or can be made to approach zero sufficiently fast as $\omega_e \to 0$ there are no particular problems, except that estimates of wave elevation in the time domain are not made.

The second general approach is to perform a numerical double integration on the acceleration, $A_v(t)$. The data samples are of 20 minute duration taken every four hours. Thus no matter what the integration method it will not be possible to produce answers for fluctuations which correspond to near zero frequency.

Accordingly, the numerical double integration may be thought of as band-pass filtering, just as in some forms of real time analog integration. Because there is no real-time requirement in the present problem, the double integration filter response function does not have to be realizable, and there is an advantage in a non-realizable filter in that incorrect phase lags need not be introduced.

The ideal filter transfer function for double integration with respect to time is:

$$H(\omega_e) = \left[\frac{-1}{\omega_e^2} + i(0)\right] \tag{45}$$

That is; the phase lag is $180^o$, independent of frequency, and the amplitude response is $1/\omega_e^2$. The time domain equivalent of Eq. (45) is symmetrical in time; that is, in order to compute the instantaneous "present" value of the double integral, as much of the "future" is required as of the "past." This is not a disadvantage in data reduction since everything the analyst has to work with has already been recorded -- at any instant in mid-sample finite amounts of "past" and "future" are known.

The obvious problem in Eq. (45) is at zero frequency, so that for any sort of practical implementation the transfer function specification must be altered to:

$$H(\omega_e) = \begin{cases} f(\omega_e) : 0 \leq \omega_e < \omega_o \\ \\ -1/\omega_e^2 : \omega_o \leq \omega_e \end{cases} \tag{46}$$

For reasons previously indicated the function $f(\omega_e)$ can be zero at $\omega_e=0$ to make the filter band-pass and must grow in some way so as to be $-1/\omega_o^2$ at $\omega_o$. The output from such a band-pass filter will be correct double integration at frequencies exceeding $\omega_o$ and quite incorrect integration for frequencies below.

The Low Frequency Cut-Off

In the initial development of the process it was assumed that a fixed low frequency cutoff would be desirable. The accelerations to be processed contain the ship's rigid body motion. The only moderately sharply tuned resonance in the ship's rigid body motion is that of roll. The ship's rolling period may vary between 20 and 30 seconds, depending upon loading. It must be assumed that even after correction for roll angle there will be at least some accelerometer output content in this range of periods, which should be handled correctly. On this basis the low frequency cutoff should correspond to encounter periods of at least 60 seconds, longer if possible.

For trial purposes, a value of $\omega_o$ of 0.0524 (120 second encounter period) was assumed and the implications with respect to double integration errors were studied in the wave frequency/heading plane. Essential results are contained in Figures 6 and 7. These are polar plots, wave frequency is along the radius and an auxiliary wave length scale is shown. The regions are shown for combinations of wave length and heading which produce roll resonance for roll periods between 20 and 30 seconds. A second pair of regions is indicated where encounter periods are greater than 120 sec. These last are the regions where double integration errors will exist for $\omega_o$ = .0524, Eq. (46).

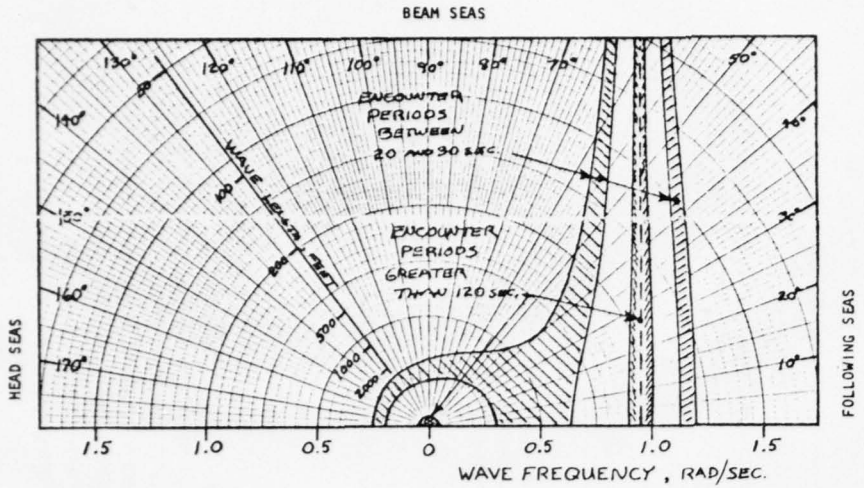


FIGURE 6 - LOCATION OF INTEGRATION ERRORS IN THE WAVE FREQUENCY/HEADING PLANE, SHIP SPEED 20 KT.

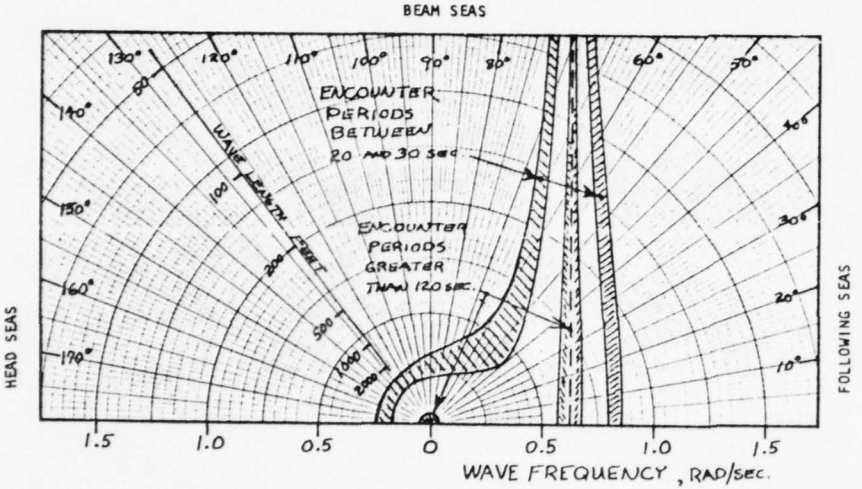


FIGURE 7 - LOCATION OF INTEGRATION ERRORS IN THE WAVE FREQUENCY/HEADING PLANE, SHIP SPEED 30 KT.

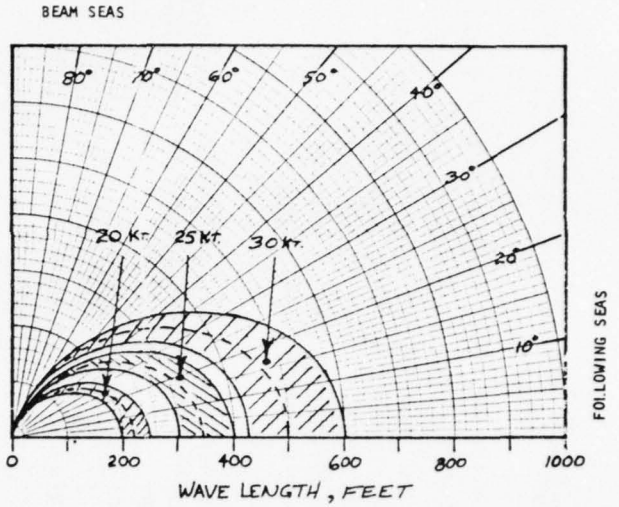


FIGURE 8 - LOCATION OF INTEGRATION ERRORS FOR QUARTERING/FOLLOWING SEAS IN THE WAVE LENGTH - HEADING PLANE

The small region of integration error around the origin is about the same size for either 20 or 30 knot ship speeds. The wave lengths involved are measured in tens of thousands of feet. According to conventional thinking, wave components of this length either do not exist or are of such small amplitude that they cannot be resolved, and thus the ship motions response to such wavelengths may be assumed negligible. On this basis no significant influence on the double integration of the low frequency cutoff may be anticipated in head through beam seas to a wave heading of around $70^{o}$.

The second region of integration error is centered around the line (shown dashed) corresponding to quartering or following wave components which travel at the ship speed. Along the dashed line in Figures 6 and 7 the encounter period is infinite ($\omega_e \approx 0$). A proper double integration is not possible with discontinuous sample records. The position of the dashed line is fixed by ship speed. The width of the error region is fixed by $\omega_o$. Considering the available experimental and theoretical ship motions results, significant ship motions (pitch, heave, roll) are not expected for waves shorter than about 1/4 ship length (say 200 feet in the present case) unless roll resonance is involved. Considering Figure 6, the second error region corresponds to waves shorter than 200 feet for quartering headings to $25^{o}$, and at worst to waves shorter than 250 feet for following seas. Serious integration errors are thus not expected for this ship speed. Similarly, Figure 7 indicates that integration errors should not be significant over headings from head to almost quartering seas ($50^{o}$) for ship speeds to 30 knots. For following/quartering seas (0 to $50^{o}$ heading) integration errors will be introduced for wave lengths which should produce ship motion. This type of error cannot be eliminated, its magnitude can only be reduced by decreasing $\omega_o$.

Figure 8 is an enlargement of the quartering/following sea error regions. In this case the radius of the plot is wave length. In the 20 to 30 knot operating speed range of the present ship, errors can be expected which correspond to the very significant (for the Atlantic) range of 300 to 600 feet wave lengths.

It seemed reasonably clear from the foregoing that the low-frequency cutoff, $\omega_o$ (Eq.46) should not exceed 0.0524 rad/sec in the present application. The widths of the bands in Figure 8 are roughly proportional to $\omega_o$ so that the influence of the integration errors for following seas should reduce in proportion. However there seemed to be little point in exerting large effort to reduce the cutoff frequency much beyond 1/2 of that assumed for Figures 6-8. For wave components of near zero encounter frequency the slant range will also vary slowly, so that the apparent period of the wave components will approach the sample length. In this circumstance there will not be anough information available to make reasonable statistical estimates about the component wave lengths in question. Nothing possible in analysis will help.

Considering the sample length of 20 minutes, component wave encounter periods of 120 to 400 seconds ($\omega_e$ = 0.0157 to .0524) involve between 3 and 10 encounter cycles in the sample. It therefore seemed a reasonable compromise for numerical development purposes to set a target cut-off of about 0.0262 rad/sec (encounter period 240 sec).

Filtering Methods - Sampled Data

By taking the Fourier transform of Eq. (46) a series of weighting coefficients may be determined so that filtering may be done with a discrete convolution of the form:

$$Z(n\Delta t) = C_o A_v(n\Delta t) + \sum_{j=1}^{P} C_j [A_v(n\Delta t - j\Delta t) + A_v(n\Delta t + j\Delta t)] \qquad (47)$$

where $\Delta t$ = sampling interval of time series

$C_j$ = weighting coefficients for non-realizable filter.

In a sample of N points, n=1,2...N, there is a starting and stopping transient (P) points in length which is only partially correct. (To compute Z(0), (P) data points for $A_v(n\Delta t)$ are required for negative n -- these points are not known.) Accordingly, it is prudent to compute $Z(n\Delta t)$ only for $(P+1) \leq n \leq (N-P)$. This has two results:

1. Results are obtained for a shorter sample. In effect the resulting time series for Z(t) is 2P points shorter than that of the original ($A_v(t)$).
2. The computing time is approximately proportional to the number of multiplications which are approximately P(N-2P).

An alternate approach is the use of "fast convolution" methods using the FFT algorithm. Broadly, in this approach the direct discrete Fourier transform of the data is taken. This results in a complex "spectrum" of the original data. The filtering is done in the frequency domain by multiplying this "spectrum" by the filter transfer function. After this operation the inverse discrete Fourier transform is taken and the result is the filtered time series in the time domain. The discrete Fourier transform has as an underlying assumption that the data is periodic in the sample length. In the present case this is not true so that an additional pre-processing step is necessary to minimize end effects. This takes the form of "tapering" or attenuating the ends of the data so that the first and last points are near zero. After the direct transform, multiplication, and inverse transforming, the result is a "tapered" rendition of the filtered data. Accordingly data at the ends of the record are also lost in the fast convolution method.

For comparison of methods the FFT method may be hypothesized in the following steps.

1. Pre-process data with the Tukey 10% cosine taper. This is a standard tapering used in FFT spectrum analysis. 10% of the data at each end of the sample is tapered so that the final results will be a time series N/5 points shorter than the original N point series. Approximate number of multiplications = N/5.

2. Do Direct FFT. Approximate number of real multiplications = 2MN where M is defined by $N=2^M$.

3. Multiply direct transform by transfer function -- 2N multiplications.

4. Do Inverse FFT -- 2MN multiplications.
   Total number of multiplications for this process is (2.2+4M)N.

The foregoing provided some basis on which to make a choice between the methods. From previous experience with digital band-pass filter coefficients of the form of Eq. (47) it was estimated that the minimum value of (P) for a reasonably precise filtering job would be about equal to the number of points necessary to define in the time domain, the period corresponding to the peak of the transfer function. Assuming the minimum acceptable period to be 120 sec or 1/10 of sample length (N), it appeared that (P) should be about 800, since the sample length for the present data is 8192.

It thus appeared that the data loss would be the same in either method -- approximately 20% of the sample length -- and no choice between the methods was dictated.

Considering computer time to be proportional to the number of real multiplications, the estimated ratio of computation times may be formed:

$$W = \frac{\text{Computation Time for Eq. (47)}}{\text{Computation Time for Fast Convolution Method}}$$

$$\approx \frac{P(N-2P)}{(2.2+4M)N}$$

Noting that $P \approx 800$ (minimum) and M=13 in the present program:

$$W \gtrsim 12$$

Thus the fast convolution method appeared to be an order of magnitude faster in the present application. Because of the large amount of data involved this speed advantage was of practical significance.

The fast convolution method was clearly the best choice. It had the further advantage that mid-way through the process nearly half of the work involved in obtaining the spectrum and cross spectrum of the vertical translation and corrected slant range (Eq.43) would be done and could be salvaged.

Preliminary Numerical Development; Fast Convolution Method

Initial trials with the fast convolution method were carried out with cosine wave inputs. Essentially a cosine wave of frequency $\omega_o$ was assumed to be the acceleration and a time series of $\cos(\omega_o j\Delta t)$ was generated for $j=0,1...(N-1)$. This series was multiplied by $-1/\omega_o^2$ to generate a "true displacement" series. The processing was carried out on the "acceleration" series and the results were compared with the "true displacement" series to assess precision.

If the sample length is an exact multiple of the periodicity of the data, the simple process of taking the inverse Fourier transform of ($-1/\omega^2$ times the Direct Fourier Transform) was found to be nearly as precise as the number of significant digits carried in the computation. However the data in question has no such restrictions about periodicity. The simple process just outlined did not result in spectacularly good precision for input periods not commensurate with sample length. In this case the fractional cycle at the end of the sample duration causes the Fourier Spectrum to be higher than it should be throughout the frequency range. Multiplication of the direct transform by $-1/\omega^2$ thus unduly emphasizes any spurious low frequency Fourier spectrum components because the spurious components arise through "leakage" of variance from the actual pure input.

With real data the exact frequency content is not known in advance and it should not be assumed that the data is free of linear trends since an appreciable linear trend also has the effect of introducing spurious leakage from high to low frequencies. Accordingly the simple process must be augmented by two pre-processing steps:

1. Correct sample to zero mean and remove linear trends in one of the standard manners. In the present case the method chosen was the minimum computation method recommended by Blackman and Tukey for spectrum analysis.
2. Perform the 10% cosine taper as recommended by Tukey to reduce "leakage." This procedure results in an effective discard of 10% of the final data at each end of the series as mentioned in a previous section. It also is one of the required steps for FFT spectrum analysis.

The incorporation of these two steps resulted in about the same precision of displacement estimates whether or not the acceleration input period was commensurate with sample duration. (For commensurate input periods the precision was degraded, for incommensurate periods it was improved.) The magnitude of rms prediction error was about 2 or 3% of displacement amplitude for periods the equivalent of 60 seconds real time. However the errors did not fall off as rapidly as was expected as period was shortened. With some simple trial and error experimentation the precision was found to be a function of the cutoff $\omega_o$, Eq. (46), and, to a much smaller degree, of the shape of $f(\omega_e)$, Eq. (46).

The reasons are purely numerical. If the input acceleration is of very high frequency the FFT acceleration spectrum has essentially noise at low frequencies. If the input frequency is high enough the $1/\omega^2$ characteristic of the filter can result in the spurious low frequency components of the acceleration spectrum being transformed into relatively significant components of the displacement spectrum. In addition, with tapering, the spectrum estimates at frequencies just below those corresponding to the lowest frequency actually present ($\omega_j$, say) correspond mostly to leakage from the lowest frequency component. The appropriate double integration multiplier for these near frequencies may consequently be $(-1/\omega_j^2)$ rather than the reciprocal of the square of the actual frequency involved.

These preliminary results with single frequency accelerations suggested that a fixed low frequency cut-off characteristic, as was originally envisioned, would not be the optimum solution for the present work. Roughly half of the present data is in nominal head or bow seas, and the other half is in nominal following or quartering seas. One constant low frequency cutoff suitable for both situations did not seem possible.

## Radar Wave Processing System

It was clear that in order to make a best estimate of doubly integrated acceleration, the acceleration spectra would have to be developed simultaneously in order to make a best choice of low frequency cutoff. Thus what initially appeared attractive to minimize computation time became a requirement. Accordingly the required (largely standard) subprogramming was gathered, the system was checked out with simulated data, and by this means a final form was developed for the double integration filter. All of the individual standard steps in the process are described in Reference 10.

The steps in the computation are as follows for each interval which was processed. (All reading and storing operations involved disk files accessible by the computer.)

1. Read the basic digitized data (slant range, roll, pitch, vertical and lateral accelerations) calibrate each channel, and compute $R_a(t)$ and $A_v(t)$ in accordance with the previous discussion. These new time series were placed in 8192 point arrays, the range in array XR and the acceleration in array XI.
2. Correct the two time series (XR,XI) for linear trends and to zero mean in accordance with the minimum computation method recommended by Blackman and Tukey (Ref.10).
3. Store the range, XR in a temporary file for later use. (When the double integration is completed the range must be retrieved in order to compute wave elevation.)
4. Apply the 10% Tukey cosine taper (Ref.10) to both the range and acceleration arrays.

5. Compute the direct fast Fourier Transform (Ref.10) of arrays XR and XI, assuming that array XR (range) is the real part and array XI (acceleration) is the imaginary part of a complex function of time. (This approach allows spectra and cross spectra to be developed later with about a 60% saving in computation time over an approach in which the spectra were developed in a separate operation.) The results of this step is a scrambled transform in arrays XR and XI -- unscrambling is a matter of simple arithmetic.

6. Store both parts of the direct transform in a second temporary file for later use.

7. Compute over-resolved scalar spectra of range and acceleration from the transform, placing the results in arrays XR and XI in the process. These spectra are defined at the minimum delta frequency possible with the given size arrays ($\Delta\omega = 2\pi/8192\ \Delta t \approx .005$ rad/sec).

8. From the over-resolved acceleration spectrum compute the parameters (to be described) of the double integration filter.

9. Read back the scrambled direct transform (XR,XI) stored in step 6.

10. Multiply the acceleration transform by the double integration filter. This was accomplished by unscrambling the range and acceleration transforms, multiplying the acceleration transform by the filter response, and then re-combining the two transforms so that the result (in arrays XR and XI) was as though the direct Fast Fourier Transform had been done with arrays containing range and displacement rather than range and acceleration.

11. From the results of step 10 compute the scalar spectra of range and displacement and the range-displacement cross-spectrum. In this step arrays XR and XI were not modified. The spectra and cross-spectrum could be placed in other smaller arrays at this stage because the final averaging over blocks of basic estimates (Ref.10) was carried out.

12. Using the results of step 11, develop the radar wave spectrum in accordance with Eq. (43), retaining for record purposes the rms corrected range $R_a(t)$ and the rms displacement.

13. Replace arrays XR and XI by the transform of displacement alone in an unscrambling step similar to that performed previously. The result is as though the direct FFT had been done with displacement in array XR and array XI zeroed.

14. Compute the inverse Fast Fourier Transform of (XR+iXI). The result is the (tapered) time history of vertical displacement in array XR.

15. Store the displacement time history for later use. (Initially this was a de-bugging step, but it was retained later for use in processing the Tucker Meter data.)

16. Read the range $R_a(t)$ from the first temporary file (step 3) into array XI.

17. Compute the wave elevation in accordance with Eq. (42) as:

$$\zeta(t) = -R_a(t) - Z_t(t)$$

$$= -XR - XI$$

18. Write out a summary file of results for the interval.

Simulation of Data for Final Development of Low Frequency Cutoff Parameters of $H(\omega_e)$

In order to develop a reasonable system for adapting the low frequency cutoff parameters of $H(\omega_e)$ to the acceleration data, a more realistic simulation of input data was in order. Because a simulation of both the acceleration and the corresponding displacement was required, the approach taken was to sum a number of co-sinusoids with incommensurate frequencies, equal amplitudes and random starting phases. Accordingly, the "true" displacement may be computed from the acceleration components. The simulated acceleration was processed. The simulated displacement was used for comparison with the results to assess precision.

In particular the simulation was as follows:

$$A_T(t) = a \sum_{j=1}^{NS} \cos(\omega_j t + \epsilon_j) \tag{48}$$

$$Z_t(t) = -a \sum_{j=1}^{NS} (1/\omega_j^2)\cos(\omega_j t + \epsilon_j) \tag{49}$$

where $a = \sigma_A \sqrt{2/NS}$

$\sigma_A$ = desired rms acceleration

NS = number of sinusoids summed

$\epsilon_j$ = random initial phase (uniform in $0 \leq \epsilon_j \leq 2\pi$)

$\omega_j$ = frequencies.

To derive the frequencies, $\omega_j$, an acceleration spectrum was assumed in the form:

$$S_A(\omega) = \frac{\pi\sigma_A^2}{2(\omega_2-\omega_1)} \sin\left[\pi \frac{\omega-\omega_1}{\omega_2-\omega_1}\right]$$

$$\omega_1 \leq \omega \leq \omega_2$$

$$= 0 \text{ elsewhere}$$

The spectrum was broken into (NS+1) equi-energy bands and the frequencies $\omega_j$ were determined by solving:

$$\frac{j\sigma^2}{NS+1} = \int_{\omega_1}^{\omega_j} S_A(\omega)\, d\omega$$

$$\text{for } j=1,2...NS$$

This procedure substantially insures incommensurate frequencies. The result, in Eq. (48), for NS=1 is a pure co-sinusoid of frequency $(\omega_1+\omega_2)/2$. As NS is increased the result begins to resemble a band-passed random function.

In virtually all the simulations using the system outlined in the last section white-noise slant range "data" with a standard deviation of 10 times that of the simulated acceleration was also simulated. Some trials were also made with zeroed simulated slant range. There appeared to be no numerical cross-talk between the slant range and acceleration.

Final Version of the Low Frequency Cutoff Parameters

The final version of the low-frequency cutoff parameters was developed more or less by trial and error. Harmonic acceleration and both narrow and wide-band "random" accelerations were processed. The results were compared with the simulated true displacement and the precision was assessed by computing the rms error over the middle 75% of the sample to eliminate the distortions induced by "tapering." This rms error was divided by the rms simulated displacement and the result, in percent, formed the basis for judgment of the adequacy of the process.

Figure 9 summarizes the final computation system chosen for $H(\omega_e)$. Given the acceleration spectrum, the acceleration variance, $\sigma_A^2$, is known. A measure of the lower limit of significant acceleration spectral density is formed by finding a frequency, $\omega_{.02}$, such that 2% of total variance is attributable to lower frequencies. This approach was chosen to avoid odd, possibly spurious, spikes in an over-resolved analysis from upsetting things.

The cutoff frequency, Eq. (46), is formed by taking 75% of $\omega_{.02}$ and adding an empirically determined term (Fig.9) which has a negligible effect on the cutoff for values of $\omega_{.02}$ which are high relative to the folding frequency. The term significantly alters the cutoff only for frequencies corresponding to fewer than 20 periods in the sample length.

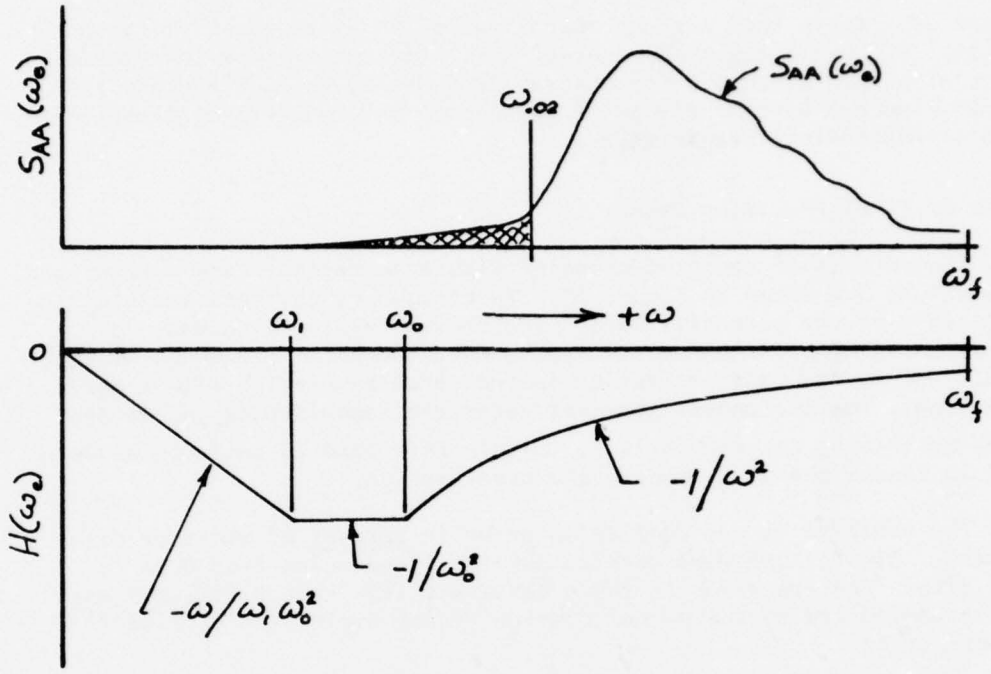


$$\sigma_A^2 = \int_0^{\omega_f} S_{AA}(\omega_e)\, d\omega_e$$

$$0.02\,\sigma_A^2 = \int_0^{\omega_{.02}} S_{AA}(\omega_e)\, d\omega_e$$

$$\omega_o = 0.75\,\omega_{.02} + 3.52\,\omega_f/N$$

$$\omega_1 = 2\,\omega_o/3$$

FIGURE 9 DEFINITION OF $H(\omega_e)$

The shape of the resulting $H(\omega_e)$ is indicated in Figure 9. The function is $(-1/\omega^2)$ above the cutoff, $\omega_o$. It is constant and equal to $(-1/\omega_o^2)$ from $(2\omega_o/3)$ to $\omega_o$, and decreases linearly to zero for lower frequencies. It is thus a rough approximation to a band-pass filter as required. Since all functions are defined in discrete steps in frequency, the actual values of cutoff frequencies used are slightly different than shown in Figure 9 by the effects of truncation in transforming frequencies to the corresponding integer steps.

Results of Final Precision Checks

The results of the processing of simulated harmonic and narrow band accelerations are shown in Figure 10. The frequency abscissa includes the entire range of the potential data. The chosen folding frequency is 3.33 Hz, the probable maximum resolvable wave encounter frequency is about 1.4 Hz. The narrow band excitation is indicated by circles with a horizontal line. The horizontal line indicates the bandwidth ($\omega_1, \omega_2$ in the section describing the simulation). Within this band 20 cosinusoids were summed in random phase to produce the acceleration.

The ordinate is rms prediction error in <u>percent</u> of rms true displacement. Simulations were carried out for frequencies from 0.08 to 0.7 Hz also. The rms error in these cases was less than 0.01%, and was probably controlled by the number of significant digits (7) carried in the computation.

In interpreting the results and developing the cutoff parameters, errors less than 1% were considered good, and the basic problem was to reduce prediction error to the order of 2% or less for frequencies of 0.008 Hz (120 sec encounter periods). Figure 10 represents about the best that could be done in this respect. It became clear that the previously mentioned target of a system good down to a 240 second encounter period could not be met. Figure 10 indicates that the basic procedure is good for encounter periods as long as 60 seconds and probably acceptable from 60 to 120 second encounter periods. For longer encounter periods larger errors develop. Their importance is outlined in Figures 6-8 and a previous section.

Figure 11 contains the results of the simulation for wide-band acceleration. The width of the acceleration spectrum is indicated by the sketch of a band-passed spectrum which serves as a plotting symbol. Each wide-band simulation was produced by summing 200 cosinusoids. Relative to Figure 10, the ordinate of Figure 11 is shifted by one decade so that the rms error for all cases is 1% or less of true rms displacement. The trend line from Figure 10 is shown. The magnitude of rms error is determined largely by the frequency of lowest significant spectral density.

In all the previous development the acceleration data input to the system had seven digit significance. This is roughly analogous to an analog instrument with a dynamic range greater than 150 db. In the present

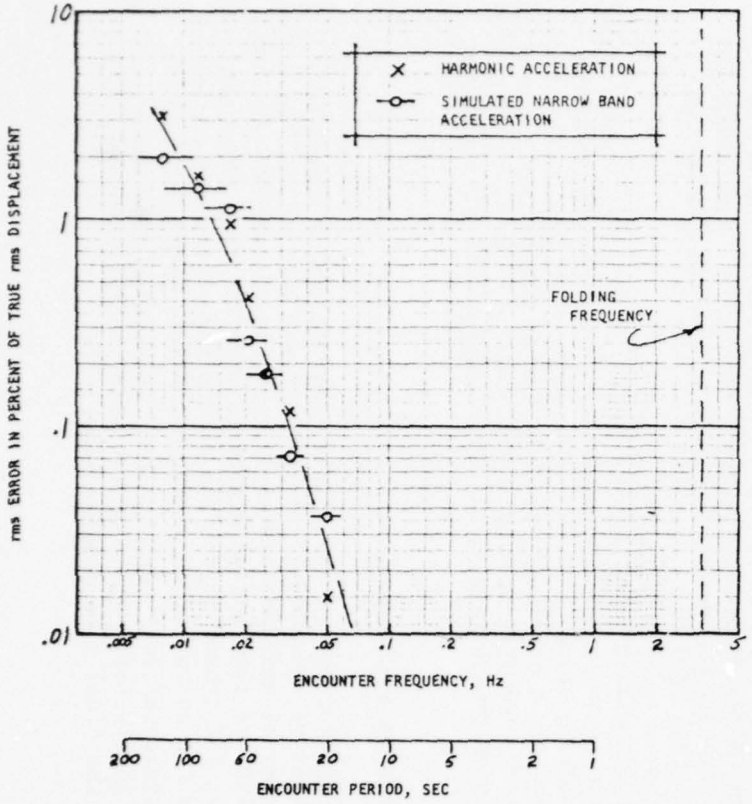


FIGURE 10 - PRECISION OF DOUBLE INTEGRATION BY FAST CONVOLUTION METHODS (HARMONIC AND NARROW BAND ACCELERATION)

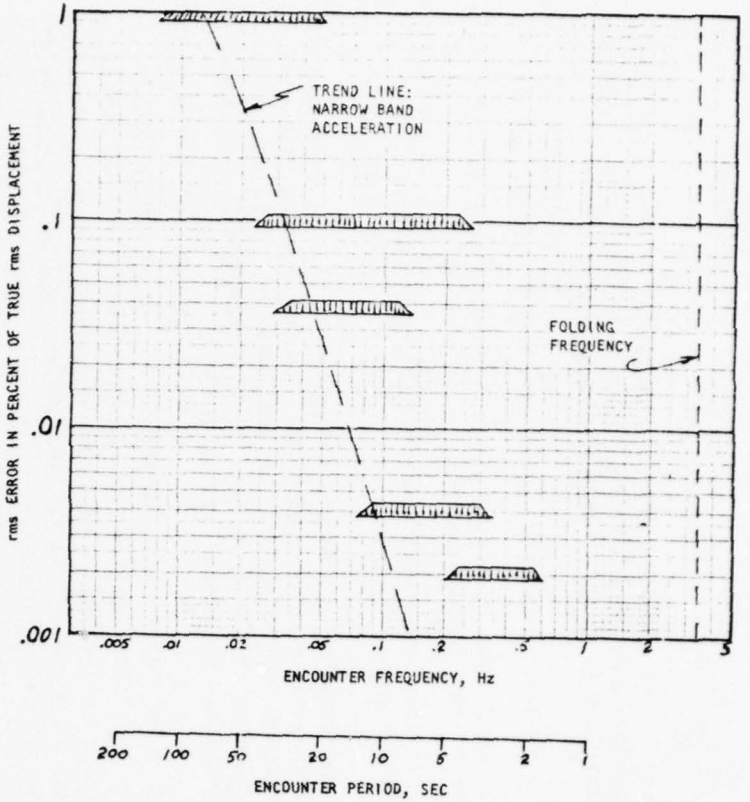


FIGURE 11 - PRECISION OF DOUBLE INTEGRATION BY FAST CONVOLUTION METHODS (WIDE BAND ACCELERATION)

case there is nothing like this dynamic range inherent anywhere in the system until the final data processing stage.

The effect of reduced significance was studied by artificially reducing the resolution of the simulated acceleration. For instance, to reduce the resolution to p% of rms acceleration $\sigma_A$:

1. The simulated acceleration was divided by $.01p\sigma_A$.
2. This result was truncated by discarding digits to the right of the decimal point.
3. Finally the last result was multiplied by $0.01p\sigma_A$ to restore scale.

Many of the simulations shown in Figures 10 and 11 were repeated with input data of various levels of significance. The results were remarkably consistent regardless of the acceleration bandwidth or frequency. The estimated precision of the double integration process involving real data may be summarized as follows:

For input acceleration data having an rms of $\sigma_A$ and which is resolved to p% of $\sigma_A$, the precision of the prediction of time domain displacement in the middle 75% of the sample appears to be as indicated in Figures 10 and 11, or equal to (.6 to 1.0)(p), whichever is greater for the frequency content involved.

In other words, if the acceleration resolution is 2% of rms acceleration, the rms error in displacement prediction is expected to be slightly less than 2% of rms displacement unless the frequencies involved are less than 0.01 Hz.

In digitizing analog magnetic tape the ±1.5 volt full scale output is (for practical reasons associated with existing hardware) resolved to about 1 part in 620 or about 0.16% of full scale. For most random processes, if the rms is in excess of 1/3 full scale, substantial saturation may be involved. Accordingly under the best possible conditions the precision of the time domain estimates of displacement will not be better than about 1/2%.

## Sample Evaluation with Actual Data

As in the development of the angular corrections to range and acceleration, extensive checking of the process was carried out for one interval. The interval was the same as that previously chosen, Run 401. Figures 12a and 12b are sample time histories obtained from the reduction of this interval. The traces at the top of the figure are the corrected range, $R_c(t)$, and the corrected acceleration, $A_v(t)$. Both traces have previously been presented in Figure 5. The "vertical displacement" in Figure 12 is the double integration of the acceleration, and the trace marked "wave" is the final time domain answer, $\zeta(t)$.

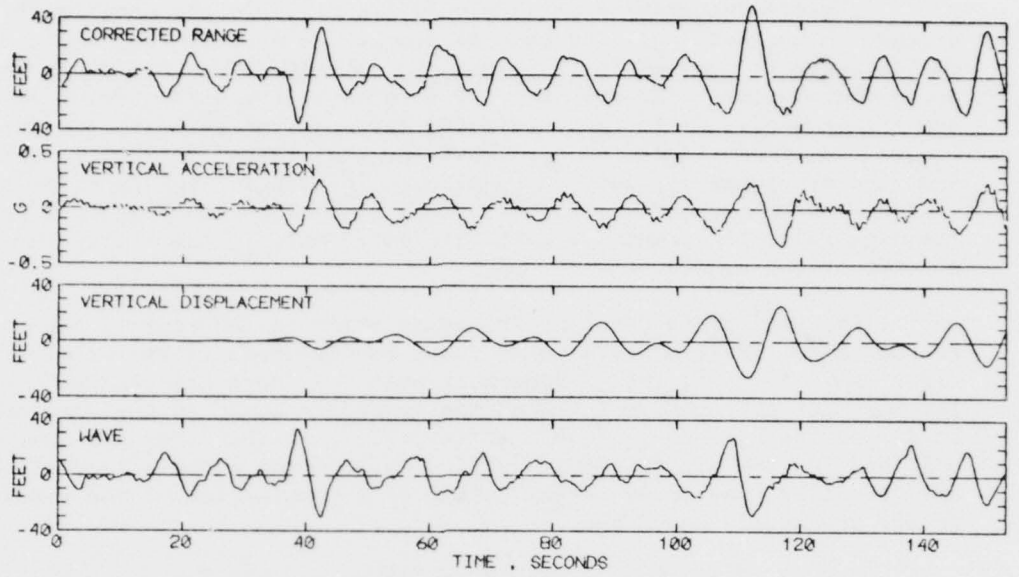


FIGURE 12a - SAMPLE RANGE, ACCELERATION, DISPLACEMENT, AND ENCOUNTERED WAVE TIME HISTORIES -- RUN 401

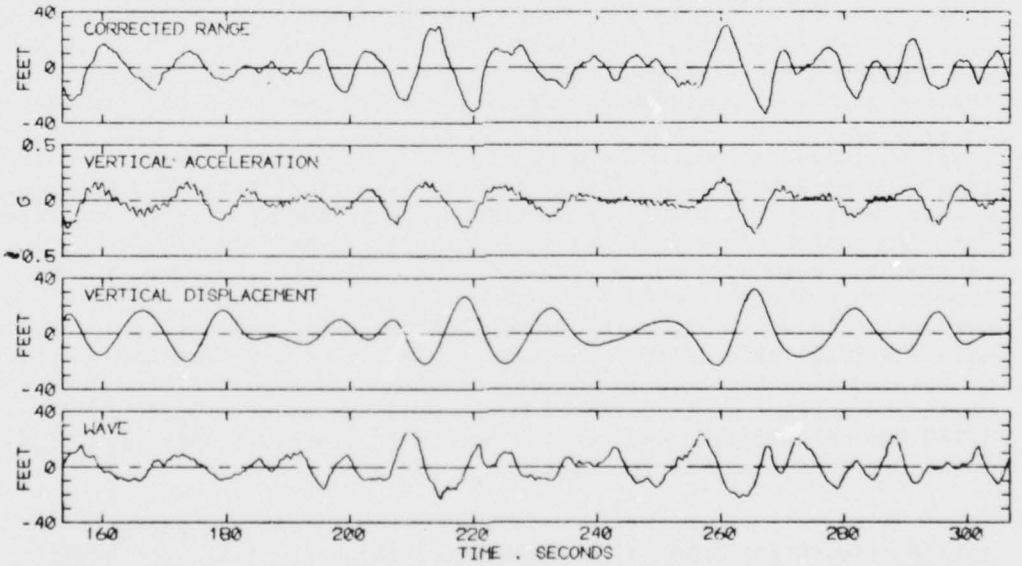


FIGURE 12b - SAMPLE RANGE, ACCELERATION, DISPLACEMENT, AND ENCOUNTERED WAVE TIME HISTORIES -- RUN 401

The displacement trace in Figure 12a displays the peculiarity brought on by tapering. The samples are 20-1/2 minutes long and the cosine taper is applied to the first and last 10% of the sample. Thus approximately the first and last 120 seconds of the displacement result are intentionally distorted. Only the last part of the displacement in Figure 12a is considered valid. Thus the wave trace (derived in part from the displacement) must be considered invalid for the first and last 2 minutes of the record so that the wave time histories resulting from the data reduction process are at best valid only in the middle 16-1/2 minutes of the sample.

The wave trace displays the noise which is inherent in the corrected range. Most of this noise seems to have been in the original slant range (Fig.5), though some must certainly have been induced by the correction process. A few of the secondary bumps in the wave trace border on the hard-to-believe. While it is felt that they are physically possible for the severe conditions involved in the example it must be admitted that they could be the result of a combination of the types of errors previously described.

Figure 13 has been prepared to illustrate the frequency domain side of the data reduction procedure for the trial interval, Run 401. At the top of the figure are plotted the spectra of corrected range, $R_a(t)$, and of the doubly integrated acceleration, $Z_t(t)$. Also indicated is the cutoff frequency, $\omega_o$, for the double integration filter. In the example virtually all of the range variance is associated with frequencies above the cutoff. From these spectra the significant double amplitude of radar range (4 x rms) is 50.3 feet, that for the vertical displacement of the radar is 42.8 feet. The radar is moving up and down almost as much as the change in its indicated range. In the middle of the figure is shown the sum of the displacement spectrum and twice the range-displacement co-spectrum. This is effectively an additive correction to the range spectrum in accordance with Eq. (43). At the bottom of the figure is the resulting wave spectrum. The correction is quite large. The significant double amplitude of wave is estimated from the spectrum to be 36.0 feet. For frequencies above 0.45 the correction indicates that range and displacement are largely out of phase so that the net (the wave) is much smaller than the corrected radar range. Below a frequency of 0.45 the correction is positive, which means that the radar was moving up and down with the local wave so that the radar range is an underestimate. If it is assumed that the ship is in long-crested head seas the frequency range where the correction is positive corresponds to waves roughly 1-1/4 to 1-1/2 the ship length, and the indication is plausible that radar and local wave are somewhat in-phase.

After all the detailed numerical checking and the analysis of sample results for internal plausibility, there is always the question about whether or not the final answer is in the "ball park." In the case of the sample interval the log-book data gives an estimated wave height of 25 feet and a swell height of 20 feet. The raw Tucker Meter wave estimate was a 13 foot significant height (4 rms). These should be compared

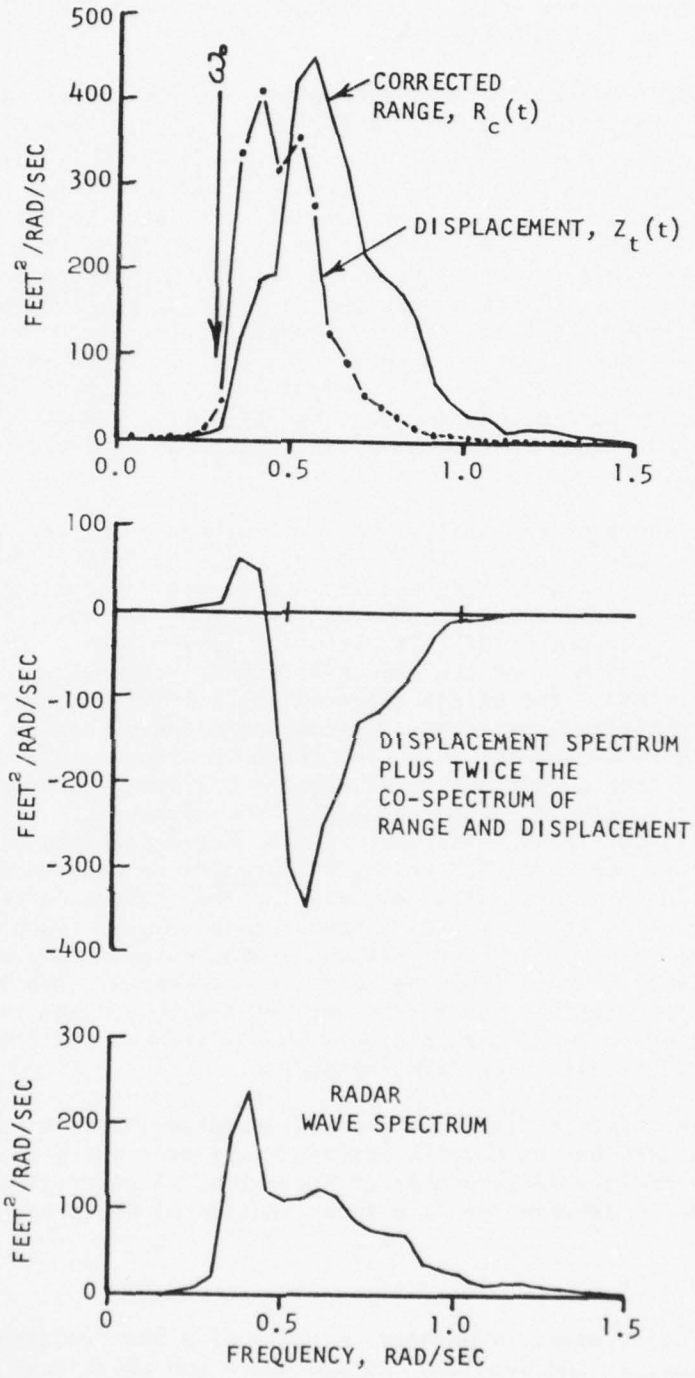


FIGURE 13 RUN 401, RADAR WAVE SPECTRUM AND COMPONENTS

with the radar wave estimate of 36 feet -- that is, the radar indication was nearly three times that of the Tucker meter, and something like 1-1/2 times the visual estimates.

On the subject of visual estimates, the interval in question was recorded at 2000 GMT, 10 January 1974, at a position roughly 43°N by 24° West, in what was described as overcast weather with rain. Local time would have been 1800 hours -- probably dark or at least twilight. The wave height at 1000 hours the same day was described as 30 feet with 15 foot swell, and that the following morning as 30-35 feet with 20 foot swell. During this period of nearly a day the ship speed was fairly consistently 12 knots or less except for an apparently brief period of trying an increased speed. It accordingly seemed permissible to speculate that the visual estimates for the interval in question could have been on the low side. If the waves during the night were not much different than in the afternoon preceding and the morning following, the comparison between visual and radar would have been 30 as opposed to 36 feet, not too bad a ballpark estimate.

In advance of the analysis of a large number of runs the above speculations were not altogether reassuring. One other simple ballpark comparison involves computing the midship longitudinal stress spectrum, dividing this by the wave spectrum derived from the radar, and taking the square root. The result of this operation (where both spectra are appreciable) is an estimate of the effective stress response amplitude per foot of wave amplitude. The stress spectrum for Run 401 was computed and the indicated operation carried out. A nominal midship section modulus was found from Reference 3 and this used to convert the result to a moment response in (foot tons/foot). The results are shown in Figure 14. The abscissa on the plot is wave frequency. Wave frequency plotting positions for the estimates from the spectral ratio were determined by assuming the ship to be proceeding at 8.7 knots into head, long crested waves. Superimposed on the plot are model test results from Reference 11 for simulated ship speeds of 25 and 30 knots in head regular waves. Considering the assumptions, the correspondence is good between the model results and the results derived in part from the radar wave spectrum. The magnitude of differences between the model test data at high speed and the ship data at relatively low speed are in line with similar results from model tests of a high speed ship shown in Reference 12.

On the basis of these results it appeared that the radar data reduction system was as checked out as it was ever going to be in advance of application to a large number of intervals. A description of the final presentation is deferred until a later section of the present report.

## Retrospective

A final summary is perhaps in order of a few fundamental problems known to exist in the data and the procedure and which have a potential for introducing errors of problematical magnitude.

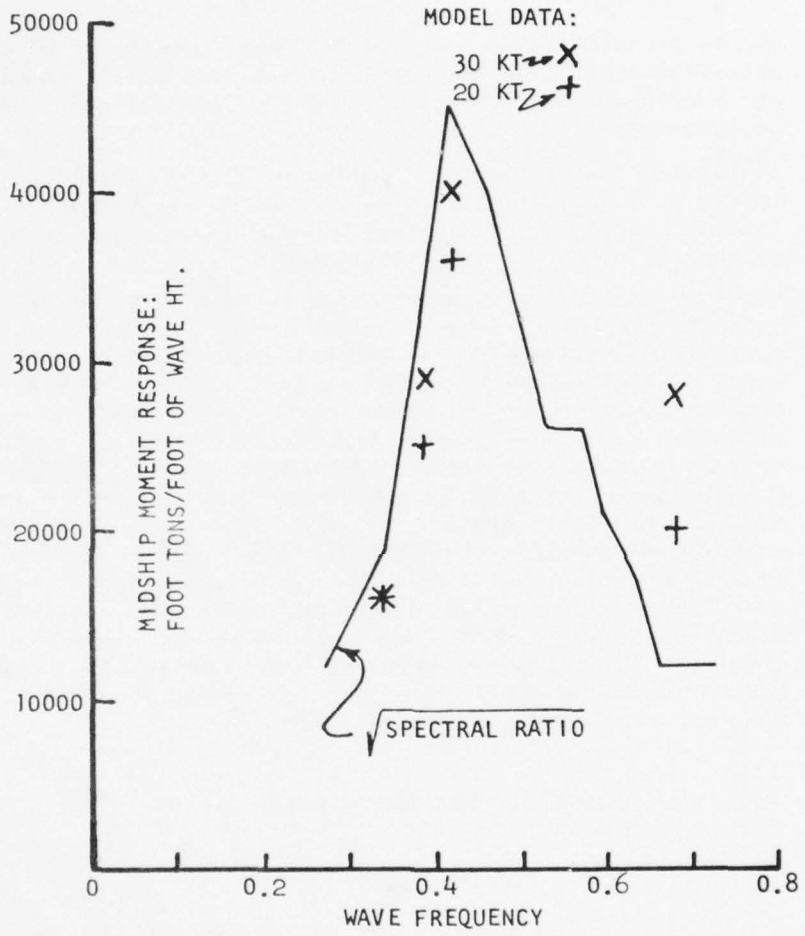


FIGURE 14 COMPARISON OF NOMINAL MIDSHIP MOMENT RESPONSE FROM SPECTRAL RATIO WITH MODEL DATA (RUN 401)

1. Loss of absolute radar range -- effects considered of probable relatively low magnitude owing to actual radar aim.

2. Angle measurements influenced by surge and sway accelerations -- effects upon estimates of true vertical acceleration considered relatively small owing to the nature of accelerometers -- effects upon vertical component of radar range considered potentially much more serious for the data involving an accelerometer package not at the position of the radar.

3. Double integration of very low frequency components of acceleration -- the lower the frequency the less well resolved the the acceleration data becomes, and the less reliable the present procedure.

4. The assumption that waves illuminated by the radar are not distorted by the ship -- there was no possible alternative to this assumption in the present work, and no impression of error from this source was attempted.

5. The fact that the spot on the free surface which is illuminated by the radar moves in a more or less sinuous path in the horizontal plane due to the lateral motions of the ship -- owing to item number 2 and the lack of yaw measurements the magnitude of this motion cannot be fully derived. However, given the actual geometry of the installation, the amplitude of such a sinuous path may be estimated as about half a ship beam at worst, an order of magnitude less than the wave lengths of most structural concern. Thus for long wave length components these effects may be considered as of less concern than others just mentioned. In the range of wave lengths less than ship beam the distortion introduced into the encountered short-wave elevations could be very large -- to the point that the physical significance of both the short period components of the derived wave elevation and the corresponding high frequency spectral densities may be questioned.

## ANALYSIS OF THE TUCKER METER

### Background

Since its introduction twenty years ago, Reference 13, there has been considerable effort (Ref.14) expended in the calibration of the "Tucker Meter" installations in the relatively small (225 foot) British weather ships. Unfortunately, full scale calibration has apparently not been carried out for larger ships (Ref.15). In the present application to a high speed ship nearly 1000 feet in length the analyst is essentially faced with a background comprising only the just mentioned references, the equipment manuals (Refs. 16,17) Pierson's analysis (Ref.7), and the computed theoretical correction curves attributed to DTNSRDC in Reference 2.

Quoting the designer of the Tucker Meter (Ref.13):

> "In principle, the instrument measures the mean height of the water surface relative to a point on the ship's hull, and adds to this the height of the point relative to an imaginary reference surface, thus giving the height of the water surface independent of vertical position of the ship."

The first height cited is measured by pressure gages mounted below the waterline, and the second is the result of doubly integrating accelerometers mounted adjacent to the pressure gages. Thus in order to produce a practical and reliable instrument within the confines of pre-1956 technology, some compromises relative to ideal design had to be made. The basic description of the instrument (Ref.13) and the rationalization of any necessary design compromise has been made almost entirely under the implied condition of zero ship speed. Indeed, the first page of Reference 13 includes the statement:

> "The ship must generally be hove-to when the recorder is in use since false wave periods will be recorded if she is moving towards or away from the waves; it has also been found by experiment that the apparent wave heights may be altered."

Effectively, what was done in calibrating the meter for the weatherships was to drop a buoy to obtain a standard wave measurement, retrieve the buoy, then record Tucker Meter output while steaming around in the area, and then finally drop the buoy again for a closing wave standard. Analysis (in Ref.14) involved deriving a directional spectrum from the buoy measurements, integrating this along various ship courses and speeds to obtain a predicted encountered wave spectrum, and then comparing the results of the derivation with the spectrum of the Tucker Meter signal. The Tucker Meter signal was assumed to be the result of cascading the true surface elevation spectrum through two filters. That is, the true spectrum $S_{\zeta\zeta}(\omega)$, was assumed to be of the form:

$$S_{\zeta\zeta}(\omega) = S_{TT}(\omega_e)/[B^2(\omega_e)\ A^2(k)] \qquad (50)$$

where

$S_{TT}(\omega_e)$ is the spectrum of the Tucker Meter Signal

$A(k)$ is a wave attenuation factor which compensates for the fact that the meter measures mean dynamic head at some depth, whereas the spectrum of the surface elevations is desired.

$B(\omega_e)$ is the known amplitude response of the double integrators built into the meter.

Effectively, if the true spectrum is known from the buoy records the factor $A(k)$ (the quantity "k" is wave number) may be estimated by:

$$A^2(k) \approx \frac{S_{TT}(\omega_e)}{S_{\zeta\zeta}(\omega_e)B^2(\omega_e)} \tag{51}$$

From simple theoretical considerations the form of A(k) is expected to be

$$A(k) = e^{-kD} \tag{52}$$

where D is the effective mean depth of the pressure recorders and k corresponds to a mean frequency. A best fit of rather badly scattered data for $1/A^2(k)$ implied D = 17.5 feet for the weathership, a value some 2-1/2 times that of the actual value of submergence of the pressure heads. This discrepancy is attributed to interference with waves by the ship. The scatter in derived values of $1/A^2(k)$ ranged up to a factor of 5, factors of 2 being typical. Use of the average correction factor on large numbers of Tucker Meter Spectra from the weatherships is regarded as being statistically correct. The results of the individual calibrations in Reference 14 imply that with the best available information the correction of any individual Tucker meter spectrum may easily result in errors in spectral area of a factor of 2. The scatter in the correction factor increased substantially with forward speed, which no-doubt led to the practice of discarding or viewing with suspicion weathership wave data obtained with the meter if ship speed was in excess of about 5 knots. The top speed in the trials analyzed in Reference 14 was 14 knots.

The computation method given in Reference 16 for the Tucker Meter response (or correction factor) incorporates in an addendum the results of the analysis of Reference 14. In effect, the wave pressure attenuation factor, Eq. (52) is computed for a depth, D, equal to 2-1/2 times the actual depth of the installed pressure sensors, and the result is multiplied by the double integrator amplitude response. The correction curves given in Reference 2 appear to have been derived in this manner.

The SL-7 Tucker Meter Installation

In the present case the Tucker Meter was installed at Frame 119, the pressure taps being located 16 feet below the 34 foot waterline port and starboard. The beam of the ship in way of the meters is 105.5 feet, and it may be noted that the Tucker Meter installation is 470 feet aft of the radar installation, and approximately 165 feet aft of midship.

The prescribed calibration procedure (Ref.17) was carried out upon installation. Though this procedure is highly detailed, one fairly important detail is omitted. This is the sense of the signal. As noted in Reference 5 no sense information was available in the calibration phase of the present project. Accordingly it was necessary to infer the sense from other channels. Of all the other channels, that with the best resolution and sensitivity to wave position is the longitudinal vertical bending stress. A positive stress is a tension in the deck, a hogging moment. From previous data as well as the SL-7 model test data (Ref.11) it is expected that a hogging moment would be in-phase with wave crest

near or aft of midship. Accordingly in the present case, positive longitudinal bending stress would be expected to be roughly in-phase with the Tucker Meter crest. In the sample time histories in References 2 and 3 and those produced for the sample run 401 previously described, positive stress and positive Tucker Meter signals were roughly out-of-phase. Thus it appeared that in the data as originally calibrated, a positive Tucker signal corresponded to a wave trough, and that the sense would have to be reversed in order to be consistent with the crest positive convention adopted for the radar. This is a simple sign reversal in the data processing.

## Analysis of Possible Corrections

In the present data set, ship speeds are usually 30 knots. Wave directions and the complexity of the wave pattern are known only to the extent of the few words in the log books. While the speed-length ratio range for the SL-7 is about the same as the range tested in the calibration of the weatherships, most of the present data involves speeds corresponding to the uppermost speed-length ratio of the weathership trials -- the situation where the scatter was worst. Though the SL-7 is four times the length of the weatherships the pressure gages are located only at twice the depth. As ships go the SL-7 is quite a different animal than the weathership.

It may be noted that in the case of the weatherships the important range of storm wavelengths in the North Atlantic (300 to $600^{+}$ feet) is entirely above the length of the ship while in the case of the SL-7 it is entirely below. Thus, for this important wavelength range the ship-wave interaction for the SL-7 would be expected to be entirely different than that for the weatherships. Many model tests in short oblique waves have shown very large attenuation of incident wave height along the ship -- relatively a much larger attenuation than is experienced in waves longer than the ship.

There seems no justification for the assumption that quantitative correction factors suitable on average for the weatherships would be applicable to the SL-7 for the prevalent wave lengths in the North Atlantic.

For initial data reduction purposes it was clear that at least the scalar spectra of the Tucker Meter signal would have to be produced. It was evident that some inspired guessing would have to be done if wave attenuation corrections of some sort were to be applied to the data, and it was decided not to attempt this in the basic data reduction procedure.

## A Study of Errors Induced by Double Integration

There are two aspects to the correction, Eq. (50). With the type of data in hand there is always the possibility of making a linear correction dependent only on encounter frequency; that is, the correction for the double integrator frequency response was theoretically feasible.

With the philosophy that half a correction might be better than none, the details of the Tucker Meter were re-examined.

After re-examining the descriptions of the system (Ref.13,16, 17) it appeared that the representation for the response of the instrument, as advanced by the designer and reflected in Eq. (50), is inconsistent with the operations which are supposed to be performed on the observations. It is claimed that the response is the product of a wave frequency response and a double integrator frequency response. When frequency response is stated in this way it means that the operations are cascaded: in the present case that the wave attenuation applies also to the displacement; and that the double integrator response applies also to the pressure head. Neither seemed true according to the stated principle of operation and the description of the system.

The above is the same point of view which was taken by Pierson (Ref.7) (though it was not so baldly stated by him), and in following up this alternate viewpoint Pierson's development in Reference 7 was followed.

Figure 15 indicates the geometry at the section where the meter is installed. A positive roll ($\varphi$) and a positive vertical displacement $Z(t)$ are indicated. The two pressure gages are located a distance D below the nominal load waterline. Associated with each gage is an accelerometer which is gymbal mounted. It appears from the descriptions, Reference 13, that the accelerations observed will be quite good approximations to true vertical accelerations. Accordingly, the quantities actually measured are pressures port and starboard ($P_p$, $P_s$) and the vertical accelerations at the same locations ($\ddot{Z}_p(t)$ and $\ddot{Z}_s(t)$). For later use, the actual static ($H_p$, $H_s$) and dynamic ($F_p$, $F_s$) heads at the location of the pressure gages are noted in the figure.

By working through hand books, References 16,17, it appeared that what is done to the measured signals by the computing circuits in the instrument may be written as follows:

$$T(t) = 1.2[P_p - D]/2 - 1.2\ell(\tau) * \ddot{Z}_p(t-\tau)/2 + 1.2[P_s - D]/2 - 1.2\ell(\tau) * \ddot{Z}_s(t-\tau)/2 \qquad (53)$$

where: $T(t)$ is the indicated wave elevation

and: $\ell(\tau)$ is the impulse response of the double integration circuits.

The asterisks in Eq. (53) denote the linear convolution operation, and the dimensions of the terms correspond to pressure head. In Eq. (53) the negative sign on the doubly integrated accelerations comes about because the displacement $Z(t)$ is here defined as positive downward, while wave (crest) is positive upward. The factor of 1.2 is a factor introduced in the calibration procedure to compensate in part for the apparent attenuation of output which is implied by the nominal computed response of the instrument.

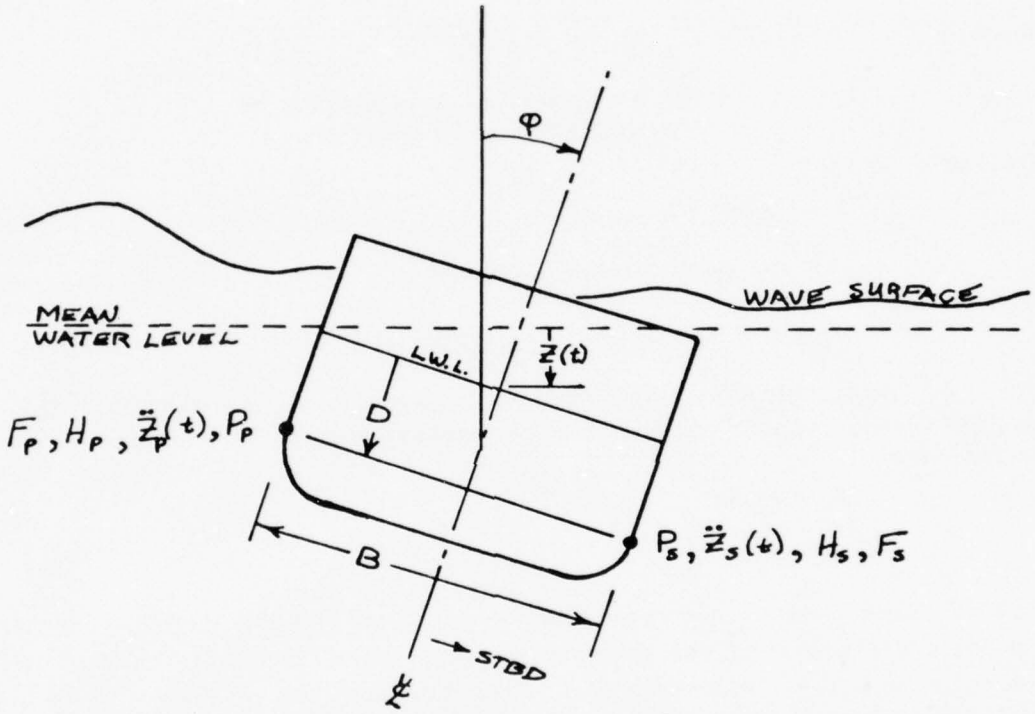


FIGURE 15 DIAGRAM OF THE TUCKER METER INSTALLATION

As may be noted, the value of Eq. (53) is zero for the case of no motions and no waves since each pressure is then just equal to static head, D. In the same way if the integrators were perfect and good to D.C., the value of Eq. (53) would also be zero for no waves and the case that the ship was given a static displacement.

Because of the accelerometer mountings mentioned and the linearity of the double integration, the two convolution terms in Eq. (53) may be replaced by:

$$-1.2\ell(\tau)*\ddot{Z}(t)$$

where:

$$\ddot{Z}(t) = [\ddot{Z}_p(t) + \ddot{Z}_s(t)]/2$$

= the mean vertical acceleration at the ship section in question.

Similarly let

$$P = [P_p + P_s]/2$$

= the mean observed pressure

Then

$$T(t) = 1.2P - 1.2D - 1.2\ell(\tau)*\ddot{Z}(t-\tau) \qquad (54)$$

Equation (54) represents what the instrument apparently does. To proceed further it was assumed that the pressures could be represented as follows:

$$P_p = F_p + H_p$$

$$P_s = F_s + H_s \qquad (55)$$

In Eqs. (55) $F_p$ and $F_s$ represent the dynamic contributions due to waves and the interference of the ship, and $H_p$ and $H_s$ are the static heads from nominal mean water. All these quantities are functions of time. It should be remarked that the arbitrary division between dynamic and static in Eq. (55) is consistent with the usual small amplitude wave theory where the total pressure at depth is the sum of a dynamic component due to waves and the hydrostatic pressure at depth. Now computing the hydrostatic heads from Figure 15 and substituting for the port and starboard pressures:

$$P = [P_p + P_s]/2$$

$$= [F_p + F_s]/2 + [H_p + H_s]/2$$

$$= [F_p + F_s]/2 + Z(t) + D\cos\varphi \qquad (56)$$

Substituting Eq. (56) into Eq. (54), the expression for the Tucker Meter signal becomes:

$$T(t) = 1.2[F_p + F_s]/2 - 1.2D[1-\cos\varphi] + 1.2Z(t) - 1.2\ell(\tau)\ast\ddot{Z}(t-\tau) \quad (57)$$

Now arbitrarily defining $F(t)$ as the mean of the dynamic heads sensed by the two pressure transducers, and rearranging Eq. (57):

$$F(t) \cong T(t)/1.2 + D\varphi^2/2 + \varepsilon(t) \quad (58)$$

with $\varepsilon(t)$ defined as:

$$\varepsilon(t) = \ell(\tau)\ast\ddot{Z}(t-\tau) - Z(t) \quad (59)$$

The approximation in the term involving D is within 1% for the range of rolling angle involved in the present data. In any event, the term $D\varphi^2/2$ would seldom exceed one foot in magnitude in the present data set. Because this term is quadratic, its contribution to fluctuations would be half a foot at most, a magnitude which must probably be considered less than the probable best accuracy of the system.

If the ship is stationary, Eqs. (58) and (59) say that the "mean dynamic head", $F(t)$, is conceptually the same as the Tucker Meter signal, $T(t)$, since it should be remembered that the factor of 1.2 arose in the calibration as a gain bias meant as an average compensation for the response of the system. If the double integration is perfect, $\varepsilon(t)$ is zero, and the "mean dynamic head" and the Tucker Meter signal differ conceptually only by a quadratic term in roll already considered largely negligible.

Equation (58) thus expresses the outcome of following the previously mentioned alternate point of view regarding the response of the instrument. The correction for double integration response appears in a quite different way. In the frequency domain, the scalar spectrum of mean dynamic head corresponding to Eq. (58) would very nearly be the sum of the spectrum of the Tucker Meter output, the spectrum of $\varepsilon(t)$, and the co-spectrum of the two terms. Presumably, the spectrum of the mean dynamic head would be corrected by a frequency dependent factor similar to $A^2(k)$ of Eq. (50) which involves only the attenuation of the waves and ship-wave interference.

It appeared worthwhile to investigate at least approximately what the integration error, $\varepsilon(t)$, Eq. (59) amounts to for present data. Taking the Fourier Transform of Eq. (59):

$$\bar{\varepsilon}(\omega) = \bar{\ddot{Z}}(\omega)[-1/\omega^2]L(\omega) - \bar{Z}(\omega) = \bar{Z}(\omega)[L(\omega) - 1] \quad (60)$$

where the bars denote the Fourier Transform. The $[-1/\omega^2]$ factor is the response of the perfect integrator. The product of this factor and the acceleration transform is the displacement transform. The (complex) function $L(\omega)$ is the response of the double integration as given in Reference 13. Relative to true displacement $L(\omega)$ is a peculiar high-pass filter in that its phases are leads at low frequency and zero at very high frequencies.

Equation (60) suggested an approach to the evaluation of $\epsilon(t)$ using the present data. In the data reduction for the radar an estimate was produced of the time history of the true vertical displacement at the forward accelerometers. This is the only vertical displacement estimate possible with the present data set. The true vertical displacement at the position of the Tucker Meter may be estimated by:

$$Z(t) = Z_{radar}(t) + 470\ \theta(t) \tag{61}$$

where $\theta(t)$ is the pitch angle, the dimensions are feet, and the plus sign results from the convention that displacements are positive down and pitch is positive bow up. Numerically, Eq. (61) is not such a good idea because pitch is small, relatively poorly resolved, and the distance between wave meters is enormous. The alternative was to do nothing.

Now with an estimate of true vertical displacement, $Z(t)$, the fast convolution method described in conjunction with the radar data reduction may be used to estimate $\epsilon(t)$, and this estimate used with the Tucker Meter data to estimate the mean dynamic head, Eq.(58).

The item not defined in the data set is the function $[L(\omega)-1]$ in Eq. (60). All that is available as a quantitative description of $L(\omega)$ is contained in Figures 5 and 6 of Reference 13. To try out the computation of $\epsilon(t)$ some reasonable interpolator function was required. Arbitrarily, the function was assumed in the form of a second order high pass filter of the form:

$$L(\omega) \approx \frac{\omega^2(\omega^2-\omega_o^2) + i\alpha\omega_o\omega^3}{(\omega_o^2-\omega^2)^2 + \alpha^2\omega_o^2\omega^2} \tag{62}$$

where $\omega_o$ = a constant cutoff frequency
$= 2\pi/T_o$

The two unknown parameters in Eq. (61) were selected so as to produce a fit to the amplitude response given in Figure 5 of Reference 14 within about 1%, and a fit to the given phase leads within $2^o$. The final values used were:

$$T_o = 31 \text{ sec}$$
$$\alpha = 1.605$$

Only a very approximate check could be made of the fit for encounter periods in excess of 50 seconds because of the nature of the graphical presentation of data in Figure 6 of Reference 13. The very low frequency behavior of the interpolator was quite reasonable relative to this latter data. Before applying the approximation to actual data, sinusoidal displacements were transformed and the results analyzed to insure that the frequency domain operator $[L(\omega)-1]$, Eq. (60) had been programmed correctly.

The procedure was applied to the interval previously selected for trial purposes, Run 401. Figures 16a and 16b are samples of the resulting time histories. The portion of data involved is the same as that shown in Figures 5 and 12. At the top is the vertical displacement at Frame 119, Eq. (61). It may be noted that the trace is noisy due to the noise in pitch, and that the first 120 seconds show the effect of tapering which is in the computed displacement at the radar. The second frame shows the hydrostatic head correction, $\epsilon(t)$, Eq. (59). This trace is also tapered as required by the fast convolution method. The third trace down is the Tucker Meter signal, calibrated and with sense reversed as previously noted. Finally, the trace at the bottom is the "mean dynamic head", Eq. (58). The term involving roll was included in the computation, but, as expected, contributed little.

The surprise in these results was how large the correction turned out to be. The results for mean dynamic head are of the same magnitude as those for the radar signal, Figure 12 (the scales are the same), whereas the Tucker signal is much smaller. What appears to produce the large correction is the combination of phases. Analysis of the study involving sinusoids indicated that the value of $\epsilon(t)$ for periods of 20 seconds should be almost as large as $Z(t)$. The magnitude of the correction shrinks to 20% of displacement for 4 sec encounter periods, and very rapidly to zero for shorter periods.

It may be noted that the hydrostatic head correction and the Tucker meter signal resemble each other and are roughly in phase. Except that the various signals were recorded at the same time on the same tape, the two traces are derived from independent measurements. For the long encounter periods of the example the phase shifts in the analog double integrators apparently results in significant error in correcting for the static head.

Under the stated conditions for Run 401 (head seas, 8.7 kt ship speed) the wave lengths corresponding to the roughly 15 to 20 second encounter periods shown range between 1-1/2 and 2 ship lengths. If this was what really existed it would be expected that the vertical displacement (heave) near midship would be roughly equal to the wave fluctuations. Figure 16 indicates that the mean dynamic head and the vertical displacement magnitudes are roughly equal, and roughly the same as the wave trace from the radar. In addition (noting that displacement in Figure 16 is positive down) the indicated wave aft of midship would be expected to slightly lag negative displacement. It is evident from the figures that this is true.

Spectra were computed for the Tucker Meter and mean dynamic head data developed for Run 401. These are shown in Figure 17 in comparison with the spectrum from the radar measurement. As noted, the significant mean dynamic head (4 rms) compares closely with that computed for the radar data. The spectral shape is different, the radar spectrum being broader. Again assuming long crested head seas, a wave attenuation correction factor was derived from Eq. (52) with D = twice the actual depth of the pressure gages, and this was applied to the mean dynamic head

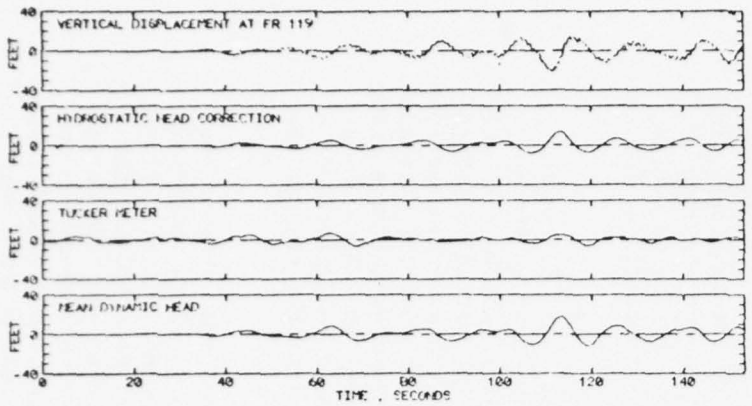


FIGURE 16a - RUN 401, SAMPLE TIME HISTORIES, TUCKER METER AND MEAN DYNAMIC HEAD

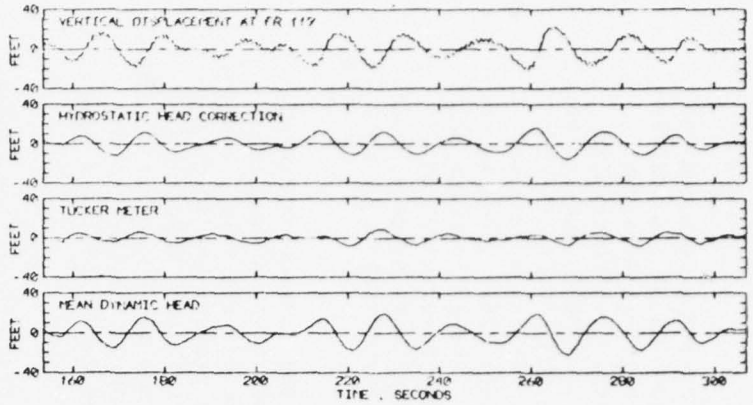


FIGURE 16b - RUN 401, SAMPLE TIME HISTORIES, TUCKER METER AND MEAN DYNAMIC HEAD

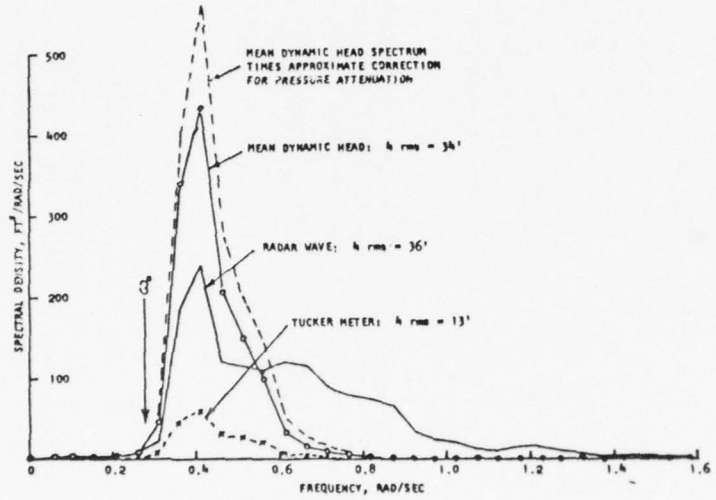


FIGURE 17 - SPECTRA DERIVED FROM TUCKER DATA (RUN 401)

spectrum. In this case the wave attenuation correction is not sufficient to align the mean dynamic head and radar spectra. The computed Tucker Meter correction curves from Reference 2 are roughly unity in the encounter range of significance in Figure 17 so that the large disparity between the basic Tucker output and the other spectra cannot be resolved in this way.

It was felt that further results for "mean dynamic head" might be of interest, and it was determined to include this in the Tucker data reduction procedure. This is of course only half a correction from another point of view. It is not known how to make the wave attenuation/interference correction to either the Tucker Meter or mean dynamic head data.

## INDIRECT METHODS OF WAVE MEASUREMENT

Because linear systems are reversible in the data reduction sense, it is tempting to attempt an inferential procedure whereby the wave spectrum is estimated from observed response spectra and the (assumed known) linear properties of the response. To illustrate the general idea and some of the more serious complications, several hypothetical cases may be formulated:

CASE 1: Ship Speed Zero, Waves Long-Crested

In this case the response and wave spectrum are simply related:

$$Y(\omega) = |H(\omega)|^2 S(\omega) \tag{63}$$

in which $H(\omega)$ is the response transfer function
$Y(\omega)$ is the observed response spectrum
and
$S(\omega)$ is the scalar) spectrum of waves.

Clearly if the response spectrum is observed and the response transfer function is known, $S(\omega)$ may be inferred. The main complication in this simple problem is that most ship response functions look like low-pass filters with a more or less strong high frequency attenuation. This means that the high frequency response spectral density tends to be driven down into the noise level of the spectral analysis method and the resulting estimate can be statistically bad.

CASE 2: Ship Speed Non-Zero, Waves Long-Crested

In this case, in general,

$$\begin{aligned} Y(\omega_e) &= |H_1(\omega_e)|^2 S_1(\omega_e) \\ &+ |H_2(\omega_e)|^2 S_2(\omega_e) \\ &+ |H_3(\omega_e)|^2 S_3(\omega_e) \end{aligned} \tag{64}$$

in which $\omega_e$ is encounter frequency

$S_i(\omega_e)$ is the encountered spectrum in region i

The encountered wave spectrum is composed of three parts, each of which has a one-to-one inverse to the wave frequency plane. Thus in the above case there are three unknown rather than 1. The solution can be approached by considering 3 responses simultaneously, thus giving 3 equations in 3 unknowns, which may be solved if the matrix of responses is not ill-conditioned.

CASE 3: Ship Speed Non-Zero, Waves Short-Crested

Here it is instructive to consider multiple responses and write down the general form of the cross and scalar spectra for responses j and k:

$$Y_{jk}(\omega_e) = \int H^*_{j1}(\omega_e) H_{k1}(\omega_e) S_1(\omega_e, X_e) dX_e + \int H^*_{j2}(\omega_e) H_{k2}(\omega_e) S_2(\omega_e, X_e) dX_e + \int H^*_{j3}(\omega_e) H_{k3}(\omega_e) S_3(\omega_e, X_e) dX_e \quad (65)$$

in the above

$Y_{jk}(\omega_e)$ = cross spectrum, responses j and k

$H_{ji}(\omega_e)$ = response j transfer function for wave mapping region i (asterisk denotes complex conjugate)

$S_i(\omega_e, X_e)$ = encountered directional wave spectrum, region i

$X_e$ = heading angle

Just as with the wave spectrum itself, all the possible response spectra and cross spectra involve the directional wave spectrum imbedded in integral equations. It is not immediately apparent if this representation can be inverted without some gross approximations about the relative wave headings. The St. Denis-Pierson model is not a conventional linear system in the encounter frequency plane.

Given that much of the present data set involves high ship speed, and that there are relatively few channels of information available, it was felt advisable not to attempt to plan on a serious attempt along the lines just discussed. For a few hove-to cases in the data set the nominal ship heading was head seas, so that there is the possibility of trying Case 1 on a few pieces of data. For this purpose the midship stress spectrum is probably the most promising response spectrum, and thus computation of the stress spectrum was indicated for the final data reduction procedure.

## THE FINAL DATA REDUCTION AND PRESENTATION PROCEDURE

The final data reduction procedure for all intervals involved:

a. Four main computation programs, the last one of which produced a complete file of results for each interval.

b. Two lister programs to supply immediate indications of some of the results.

c. One file consolidation program which produced one file for each voyage leg containing everything but the time histories of radar wave and mean dynamic head.

d. Two programs to generate the final graphical presentations for each interval.

Items b through d amount to bookkeeping operations. The work is done in the four main computation programs.

The first computation program carried out the procedure previously described for the radar. At its conclusion the radar wave spectrum and the computed time history were written in temporary files as was the time history of vertical displacement at the radar.

The second program involved reduction of the Tucker data. Both the original data and the displacement file produced by the first program were accessed. The procedure described was carried out so that time histories of mean dynamic head and the Tucker Meter signal were available. These were spectrum analyzed, and all results written in a temporary file.

The third computation program accessed the various wave-related time histories (radar, Tucker, and mean dynamic head) and performed a peak-trough analysis on the middle 16-1/2 minutes of each. (Because of the previously described tapering both the radar and mean dynamic head data are not valid for the first and last two minutes of sample.) The object of the peak-trough analysis was to produce double amplitude statistics. The zero crossing convention was used; that is, a crest was defined as the largest instantaneous value in an excursion above the sample mean, a trough was the smallest instantaneous value in an excursion below the sample mean. The double amplitude is the difference in elevation between crest and succeeding trough. In this approach small fluctuations are more or less ignored if they are riding on top of large ones. The results resemble the double amplitudes which would be estimated by hand from an oscillograph record except that the hand analyst would probably visually fair through superimposed noise whereas the computer does not. The effect is that while the computer gets about the same number of double amplitudes as the human analyst, the computer's answers tend to be higher if the records are noisy. From the double amplitudes found the average of 1/3 and 1/10 highest were computed, and the position in the sample of the largest double amplitude was noted. All results, including the actual double amplitudes were written in a temporary file.

The fourth computation program accessed the original data and performed spectrum analyses upon the midship vertical bending stress and roll. It then accessed all previously written temporary files and produced a new file containing all of the results for the interval. These results included log-book data, results of the first analysis of raw data (Ref.5), five spectra along with all analysis parameters, all results from the peak-trough analysis, and the two new time histories, the radar wave and the mean dynamic head. These files were meant to be stored on magnetic tape for possible future reference.

The final presentation of results for each interval is contained on two charts. Sample charts for the example interval used throughout this report are included as Figures 18 and 19. The first of the two charts contains the scalar spectra and a tabulation of results. The second chart involves sample time histories. Both are identified at the bottom with the DL run number, the voyage number, the analog tape and interval numbers, and the index number assigned by Teledyne.

Referring to Figure 18, the tabulation at the left is intended as a summary of the most significant numbers pertaining to the interval. At the top is as much of the original log-book data as it seemed reasonable to squeeze in. This includes date, time, position, and ship speed, as well as the visual estimates of wave and swell heights and directions. Directions are counted from the bow to port or starboard in degrees. The "sea state" is apparently the Beaufort wind. The final line in the first section of the tabulation includes comments on visual weather and, after the slash, any other comment appearing in the log.

The second box in the tabulation involves midship longitudinal stress results. Only two of the many numbers which are available could be included as indices. The first is the maximum peak to trough stress excursion as obtained in Reference 2. The second index is the significant stress (4 times rms) as derived from the area of the stress spectrum obtained in the present reduction.

The third box in the tabulation is a summary of motions. Again the "significant" motions (4 rms) are indicated. The value for roll was derived from spectrum area, that for pitch and accelerations from the rms of the basic data. (Unless there are significant linear trends in the data the differences are slight between "raw" and "spectrum" rms.) The last three items in the list involve various stages in the radar data reduction. The first is the slant range as recorded. The "vertical range" is $R_c(t)$ of the radar analysis. This entry is essentially the vertical component of the range relative to the position of the accelerometer package. The number was derived from the spectrum. The last entry is the significant displacement at the radar (significant doubly integrated acceleration). It too was derived from spectrum analyses.

In a sense, the table at the bottom of the tabulation contains the final numerical answers. Items in the first column pertain to the uncorrected Tucker Meter signal. The second column pertains to the mean dynamic

| LOG BOOK DATA | |
|---|---|
| DATE AND TIME | 01-10-74 2000 |
| POSITION | 43-29 N 24-51 W |
| COURSE AND SPEED | 250 , 8.7 KNOTS |
| SEA STATE | 9 |
| WAVE HEIGHT | 25 FEET |
| " REL DIR | 20 STBD |
| SWELL HEIGHT | 20 FEET |
| " REL DIR | 20 STBD |

---- VISUAL WEATHER / COMMENTS ----

OCAST RAIN /

| MIDSHIP VERTICAL BENDING STRESS | |
|---|---|
| MAXIMUM PK-TR | 19.4 KPSI |
| 4.0 X RMS | 11.4 KPSI |

| SUMMARY OF MOTIONS (4.0 X RMS) | |
|---|---|
| ROLL | 23.6 DEG |
| PITCH | 1.67 DEG |
| DK HSE VERT ACCEL | 0.38 G |
| DK HSE LAT ACCEL | 0.62 G |
| RADAR SLANT RANGE | 60.1 FEET |
| VERTICAL RANGE | 50.3 FEET |
| DISPL AT RADAR | 42.8 FEET |

WAVE HEIGHT STATISTICS (FEET)

| | TUCKER/DYN. | HEAD/RADAR | |
|---|---|---|---|
| P-T SAMPLE SIZE | 95 | 70 | 125 |
| MAXIMUM HEIGHT | 17.6 | 46.8 | 49.1 |
| 10TH HIGHEST HTS | 14.7 | 38.7 | 41.0 |
| 3RD HIGHEST HTS | 12.0 | 31.8 | 33.4 |
| 4.0 RMS(SPECTRA) | 13.2 | 33.5 | 36.0 |

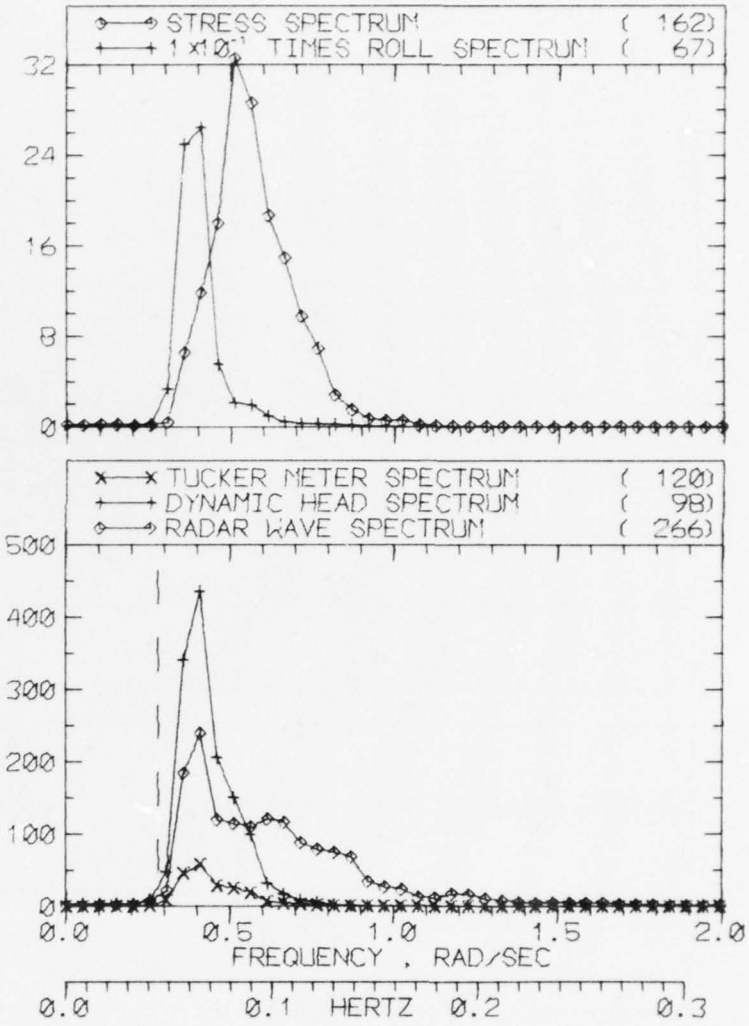


RUN 401 -- VOYAGE 32W -- TAPE 145 -- INDEX 17 -- INTERVAL 1

FIGURE 18

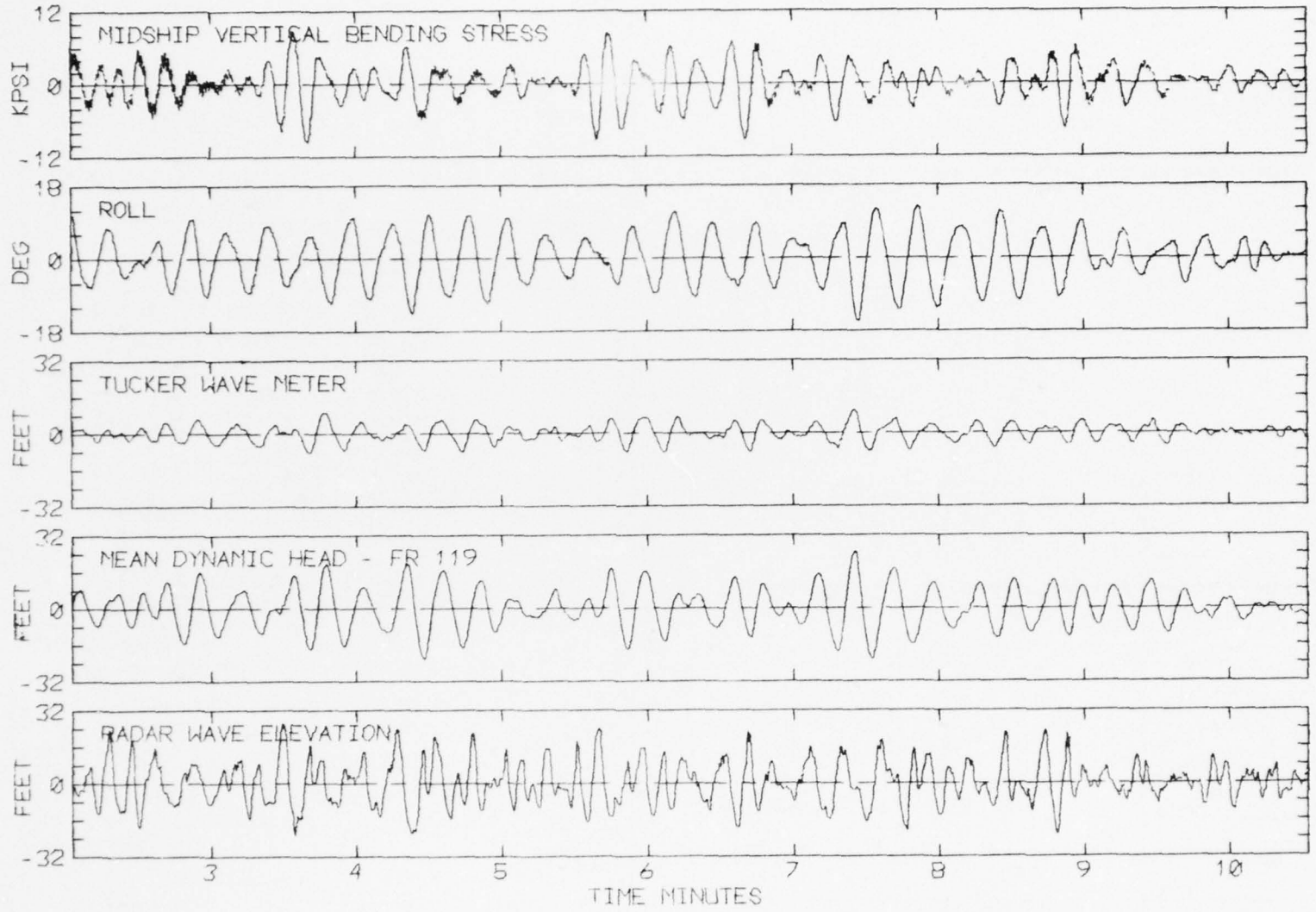


RUN 401 -- VOYAGE 32W -- TAPE 145 -- INDEX 17 -- INTERVAL 1

FIGURE 19

head developed in conjunction with the analysis of the Tucker meter, and the third column pertains to wave elevations derived from the radar system. The first row in the table is the number of double amplitudes found in the middle 16-1/2 minutes of the sample. Below this are noted the maximum height found and the averages of the 1/10 and 1/3 highest double amplitudes. The final line in the table is the significant (4 rms) height derived from the spectral analyses. Ordinarily it is expected that the last two lines of the table will be about the same.

At the right of Figure 18 are plots of the five computed spectra. It was decided to standardize the frequency scale from 0 to 2 rad/sec. In the great majority of intervals everything of interest is contained in this range. In some intervals one spectrum or another is non-negligible beyond 2 rad/sec but nothing much has been seen beyond 2.5 rad/sec for any of the quantities analyzed except in the stress spectrum where something may often be noticed around the frequency of the first mode of vertical vibration. The folding frequency of the analyses is above 20 rad/sec; no aliasing is expected, Reference 5.

The stress and roll spectra are plotted together. The vertical scale is for the stress spectrum. The roll spectrum has been multiplied by the factor noted in the legend before plotting. Dimensions of the stress spectral density are ($kpsi^2$/rad/sec) and those of the roll spectral density are ($deg^2$/rad/sec).

All three wave related spectra (Tucker, mean dynamic head, and radar) are plotted together to the same scale. The dimension of the wave spectral density is ($feet^2$/rad/sec). In the wave spectrum plot there is a vertical (slightly joggled) dashed line. This line marks the position of the low frequency cutoff, $\omega_o$, discussed previously in conjunction with double integration of the vertical accelerations. It is correct to interpret the position of this line as meaning that the double integration has been done correctly for higher frequencies, and incorrectly for lower frequencies.

There are several details about the spectrum analyses which are not documented in the plots because they are constant throughout the data reduction. First, the normalization of the spectra is such that the spectrum area equals variance. All spectra are derived from a Fast Fourier Transform analysis of an 8192 point sample. The fundamental result is 4096 spectral estimates of 2 degrees of freedom each. These estimates are uniformly spaced in frequency at a delta-frequency of 0.00511 rad/sec. In order to improve statistical reliability the basic spectral estimates were averaged in blocks of 20 estimates at intervals of 10 estimates. The resulting averages are thus equi-spaced on the frequency scale at intervals of $\Delta\omega$ = 0.0511 rad/sec. This also means that adjacent spectral estimates as shown in the plot are not quite independent -- to about the same degree as spectral estimates from the older autocorrelation methods are not independent.

As a result of the averaging, each spectral estimate has 40 degrees of freedom associated with it. Accordingly, the 90% confidence bounds on the spectra shown in the charts may be formed by multiplying the values given by 0.72 and 1.51. Had the process sampled continued indefinitely and a large number of 20.5 minute samples been obtained and analyzed, nine out of ten of these new estimates of spectral density would be expected to lie within the bounds so constructed. The practical implication is simply that the influence of sampling variability upon the given numerical results is roughly the same as that associated with the result of most other full scale wave measurement exercises.

The last detail of the spectrum analysis is the "total degrees of freedom" Reference 10. This number is included in parentheses at the end of each line of legend because it depends upon the shape of each individual spectrum. It is an estimate of the proper number of degrees of freedom to use in constructing confidence bounds on the sample variance. If each of the numbers in the present 8192 point time histories had been picked randomly the "total degrees of freedom" would be 8191. This is not the case -- adjacent members of all the present time series are highly correlated so that the equivalent "random" sample size is much smaller. In the present data set the "total degrees of freedom" (TDF) is expected to vary between 60 and 600. Approximate 90% confidence bounds on the variances assuming a Normal zero mean process, may be constructed by multiplying the estimate by two factors derived from the percentage points of the Chi-square distribution. Examples of the values of these factors are given as follows:

| TDF | Factor for Lower Bound | Factor for High Bound |
|---|---|---|
| 60 | .72 | 1.32 |
| 120 | .80 | 1.27 |
| 200 | .84 | 1.17 |
| 400 | .89 | 1.12 |
| 600 | .91 | 1.10 |

These are factors for the variances. The square root applies to the rms values so that very roughly the 90% confidence bounds on rms range from the sample rms ± 15% for TDF = 60 to the sample rms ± 5% for TDF = 600. The practical implications of these results are quite similar to those mentioned in connection with the confidence bounds on the spectra. There is only so much "precision" obtainable from one 20 minute sample of wave elevation -- that which was attained in the present work appears comparable to that achieved in the past in similar studies. With respect to comparisons between wave meters or between data and predictions of rms ship responses there can be little justification to a concern about differences of 5 to 15% magnitude.

Figure 19, the sample time histories, needs little explanation, except perhaps to say that the duration of the sample shown (8-1/2 minutes) was a compromise between a desire to display as much of the 16-1/2 minutes

of derived wave time histories as was possible in one page; and the desire to spread the time scale out so that individual fluctuations were visible for intervals involving high ship speed in head seas. To produce the charts an 8-1/2 minute portion of the available 16-1/2 minutes of sample was chosen such that the largest radar wave double amplitude is shown -- as well as (if possible) the largest mean dynamic head double amplitude.

It may be fairly asked why the effort in producing plotted time histories for each interval was considered worthwhile. The answer to the question is fairly simple. While the present data in its original analog form has been scanned systematically by eye (Refs. 2,3,5), the process involved oscillograph records with a time scale of about 15 minutes to the inch. At this time compression only a gross idea of what was happening can be formed, no detailed assessment of the believability of the data can be made, and, most importantly, the odd malfunction which is enough to upset the spectrum estimates or the statistics may often go unnoticed. This last is considered most important in the radar data. It was pointed out earlier and in Reference 5 that an attempt was made to weed out intervals where the radar had evidently lost signal and re-established a new reference range. In this process only the most obvious instances could be identified; no guarantees could be made that all instances of moderate or small magnitude had been eliminated.

## REFERENCES


1. Fain, R.A., "Design and Installation of a Ship Response Instrumentation System Aboard the SL-7 Class S.S. SEA-LAND McLEAN," SSC-238, SL-7-1, 1973, AD-780090.

2. Wheaton, J.W. and Boentgen, R.R., "Second Season Results from Ship Response Instrumentation Aboard the SL-7 Class Containership S.S. SEA-LAND McLEAN in North Atlantic Service," SL-7-9, 1976, AD-A034162.

3. Boentgen, R.R., "Third Season Results from Ship Response Instrumentation Aboard the SL-7 Class Containership S.S. SEA-LAND McLEAN in North Atlantic Service," SL-7-10, 1976, AD-A034175.

4. Johnson, A.E., Flaherty, J.A. and Walters, I.J., "A Method for Digitizing, Preparing and Using Library Tapes of Ship Stress and Environment Data," SSC-236, 1973.

5. Dalzell, J.F., "Original Radar and Standard Tucker Wavemeter SL-7 Containership Data Reduction and Correlation Sample," SL-7-14, 1978.
SSC-277.

6. St.Denis, M. and Pierson, W.J., "On the Motions of Ships in Confused Seas," SNAME 61, pp. 280, 1963.

7. Pierson, W.J., "On the Phases of the Motions of Ships in Confused Seas," Technical Report No. 9, Nonr-285(17), New York University, 1957.

8. Chen, D. and Hammond, D., "A Report on Shipboard Wave Height Radar System," Naval Research Laboratory, January 1976.

9. "Nomenclature for Treating the Motion of a Submerged Body Through a Fluid," SNAME, T. & R. Bulletin No. 1-5, April 1950.

10. Bendat, J.S. and Piersol, A.G., "Random Data: Analysis and Measurement Procedures," John Wiley & Sons, New York, 1971.

11. Dalzell, J.F. and Chiocco, M.J., "Wave Loads in a Model of the SL-7 Containership Running at Oblique Headings in Regular Waves," SSC-239, SL-7-2, 1974, AD-780065.

12. Dalzell, J.F., "Cross Spectral Analysis of Ship Model Motions: A Destroyer Model in Irregular Long-Crested Head Seas," Davidson Laboratory Report 810, Stevens Institute of Technology, April 1962.

13. Tucker, M.J., "A Shipborne Wave Recorder," Transactions RINA, Vol. 98, 1956, pp.236.

14. Cartwright, D.E., "The Use of Directional Spectra in Studying the Output of a Wave Recorder on a Moving Ship," Ocean Wave Spectra (Proceedings of a Conference), Prentice-Hall, Inc., 1963.

15. Sellers, F.H., "The Dynamic Calibration of Shipborne Wave Gages," Report No. 67-11, Department of Naval Architecture, Massachusetts Institute of Technology, July 1967.

16. "Handbook for the Shipborne Wave Recorder," Handbook Reference H.11, National Institute of Oceanography, January 1961.

17. "Handbook for the Calibration of the Shipborne Wave Recorder," Handbook Reference H 8, National Institute of Oceanography.

UNCLASSIFIED

SECURITY CLASSIFICATION OF THIS PAGE (When Data Entered)

| REPORT DOCUMENTATION PAGE | | READ INSTRUCTIONS BEFORE COMPLETING FORM |
|---|---|---|
| 1. REPORT NUMBER<br>SSC-278 (SL-7-15) | 2. GOVT ACCESSION NO. | 3. RECIPIENT'S CATALOG NUMBER |
| 4. TITLE (and Subtitle)<br>WAVEMETER DATA REDUCTION METHOD AND INITIAL DATA FOR THE SL-7 CONTAINERSHIP | | 5. TYPE OF REPORT & PERIOD COVERED<br>Technical Report<br>6. PERFORMING ORG. REPORT NUMBER |
| 7. AUTHOR(s)<br>J. F. DALZELL | | 8. CONTRACT OR GRANT NUMBER(s)<br>N00024-74-C-5451 |
| 9. PERFORMING ORGANIZATION NAME AND ADDRESS<br>Stevens Institute of Technology<br>Hoboken, N.J. | | 10. PROGRAM ELEMENT, PROJECT, TASK AREA & WORK UNIT NUMBERS<br>Task 17593 |
| 11. CONTROLLING OFFICE NAME AND ADDRESS<br>Department of the Navy<br>Naval Ship Engineering Center<br>Washington, D.C. 20362 | | 12. REPORT DATE<br>June 1978<br>13. NUMBER OF PAGES<br>68 |
| 14. MONITORING AGENCY NAME & ADDRESS(if different from Controlling Office)<br>Ship Structure Committee<br>U.S. Coast Guard Headquarters<br>Washington, D.C. 20590 | | 15. SECURITY CLASS. (of this report)<br>UNCLASSIFIED<br>15a. DECLASSIFICATION/DOWNGRADING SCHEDULE |
| 16. DISTRIBUTION STATEMENT (of this Report)<br>UNLIMITED | | DISTRIBUTION STATEMENT A<br>Approved for public release;<br>Distribution Unlimited |
| 17. DISTRIBUTION STATEMENT (of the abstract entered in Block 20, if different from Report)<br>UNLIMITED | | |
| 18. SUPPLEMENTARY NOTES | | |
| 19. KEY WORDS (Continue on reverse side if necessary and identify by block number) | | |


20. ABSTRACT (Continue on reverse side if necessary and identify by block number)

So that more precise correlations between full scale observations and analytical and model results could be carried out, one of the objectives of the instrumentation program for the SL-7 class container ships was the provision of instrumental measures of the wave environment. To this end, two wave meter systems were installed on the S.S. SEA-LAND McLEAN. Raw data was collected from both systems during the second (1973-1974) and third (1974-1975) winter data collecting seasons. → next page


DD FORM 1 JAN 73 1473 EDITION OF 1 NOV 65 IS OBSOLETE
S/N 0102-014-6601

UNCLASSIFIED

SECURITY CLASSIFICATION OF THIS PAGE (When Data Entered)

It was the purpose of the present work to reduce this raw data, to develop and implement such corrections as were found necessary and feasible, and to correlate and evaluate the final results from the two wave meters. In carrying out this work it was necessary to at least partly reduce several other channels of recorded data, so that, as a by-product, reduced results were also obtained for midship bending stresses, roll, pitch, and two components of acceleration on the ship's bridge.

As the work progressed it became evident that the volume of documentation required would grow beyond the usual dimensions of a single technical report. For this reason the analyses, the methods, the detailed results, discussions, and conclusions are contained in a series of ten related reports.

This report documents some background analyses, as well as those which were necessary to develop the needed corrections to the raw digitized data. Implementation of the results of the various analyses in a second data reduction stage is discussed.

# METRIC CONVERSION FACTORS

## Approximate Conversions to Metric Measures

| Symbol | When You Know | Multiply by | To Find | Symbol |
|---|---|---|---|---|
| | **LENGTH** | | | |
| in | inches | *2.5 | centimeters | cm |
| ft | feet | 30 | centimeters | cm |
| yd | yards | 0.9 | meters | m |
| mi | miles | 1.6 | kilometers | km |
| | **AREA** | | | |
| $in^2$ | square inches | 6.5 | square centimeters | $cm^2$ |
| $ft^2$ | square feet | 0.09 | square meters | $m^2$ |
| $yd^2$ | square yards | 0.8 | square meters | $m^2$ |
| $mi^2$ | square miles | 2.6 | square kilometers | $km^2$ |
| | acres | 0.4 | hectares | ha |
| | **MASS (weight)** | | | |
| oz | ounces | 28 | grams | g |
| lb | pounds | 0.45 | kilograms | kg |
| | short tons (2000 lb) | 0.9 | tonnes | t |
| | **VOLUME** | | | |
| tsp | teaspoons | 5 | milliliters | ml |
| Tbsp | tablespoons | 15 | milliliters | ml |
| fl oz | fluid ounces | 30 | milliliters | ml |
| c | cups | 0.24 | liters | l |
| pt | pints | 0.47 | liters | l |
| qt | quarts | 0.95 | liters | l |
| gal | gallons | 3.8 | liters | l |
| $ft^3$ | cubic feet | 0.03 | cubic meters | $m^3$ |
| $yd^3$ | cubic yards | 0.76 | cubic meters | $m^3$ |
| | **TEMPERATURE (exact)** | | | |
| °F | Fahrenheit temperature | 5/9 (after subtracting 32) | Celsius temperature | °C |

*1 in. = 2.54 (exactly). For other exact conversions and more detailed tables, see NBS Misc. Publ. 286, Units of Weights and Measures. Price $2.25, SD Catalog No. C13.10:286.


## Approximate Conversions from Metric Measures

| Symbol | When You Know | Multiply by | To Find | Symbol |
|---|---|---|---|---|
| | **LENGTH** | | | |
| mm | millimeters | 0.04 | inches | in |
| cm | centimeters | 0.4 | inches | in |
| m | meters | 3.3 | feet | ft |
| m | meters | 1.1 | yards | yd |
| km | kilometers | 0.6 | miles | mi |
| | **AREA** | | | |
| $cm^2$ | square centimeters | 0.16 | square inches | $in^2$ |
| $m^2$ | square meters | 1.2 | square yards | $yd^2$ |
| $km^2$ | square kilometers | 0.4 | square miles | $mi^2$ |
| ha | hectares (10,000 $m^2$) | 2.5 | acres | |
| | **MASS (weight)** | | | |
| g | grams | 0.035 | ounces | oz |
| kg | kilograms | 2.2 | pounds | lb |
| t | tonnes (1000 kg) | 1.1 | short tons | |
| | **VOLUME** | | | |
| ml | milliliters | 0.03 | fluid ounces | fl oz |
| l | liters | 2.1 | pints | pt |
| l | liters | 1.06 | quarts | qt |
| l | liters | 0.26 | gallons | gal |
| $m^3$ | cubic meters | 35 | cubic feet | $ft^3$ |
| $m^3$ | cubic meters | 1.3 | cubic yards | $yd^3$ |
| | **TEMPERATURE (exact)** | | | |
| °C | Celsius temperature | 9/5 (then add 32) | Fahrenheit temperature | °F |

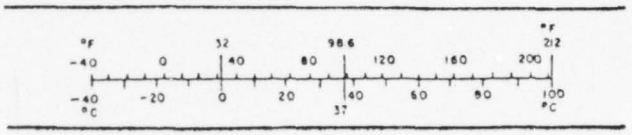


* U.S. GOVERNMENT PRINTING OFFICE : 1978 O-726-963/587

SHIP RESEARCH COMMITTEE
Maritime Transportation Research Board
National Academy of Sciences-National Research Council

The Ship Research Committee has technical cognizance of the interagency Ship Structure Committee's research program:

MR. O. H. OAKLEY, Chairman, *Consultant, McLean, Virginia*
MR. M. D. BURKHART, *Head, Marine Science Affairs, Office of Oceanographer of the Navy*
DR. J. N. CORDEA, *Senior Staff Metallurgist, ARMCO Steel Corporation*
MR. D. P. COURTSAL, *Vice President, DRAVO Corporation*
MR. E. S. DILLON, *Consultant, Silver Spring, Maryland*
DEAN D. C. DRUCKER, *College of Engineering, University of Illinois*
MR. W. J. LANE, *Consultant, Baltimore, Maryland*
DR. W. R. PORTER, *Vice Pres. for Academic Affairs, State Univ. of N.Y. Maritime College*
MR. R. W. RUMKE, *Executive Secretary, Ship Research Committee*

The Ship Design, Response, and Load Criteria Advisory Group prepared the project prospectus, evaluated the proposals for this project, provided the liaison technical guidance, and reviewed the project reports with the investigator:

MR. W. J. LANE, Chairman, *Consultant, Baltimore, Maryland*
PROF. A. H.-S. ANG, *Dept. of Civil Engineering, University of Illinois*
PROF. S. H. CRANDALL, *Dept. of Mechanical Engineering, Massachusetts Institute of Technology*
DR. M. K. OCHI, *Research Scientist, Naval Ship R & D Center, Bethesda, MD*
PROF. W. D. PILKEY, *Dept. of Mechanics, University of Virginia*
PROF. R. H. SCANLAN, *Dept. of Civil & Geological Engrg., Princeton University*
PROF. H. E. SHEETS, *Chairman, Dept. of Ocean Engrg., University of Rhode Island*
MR. H. S. TOWNSEND, *Consultant, Westport, Connecticut*

## SHIP STRUCTURE COMMITTEE PUBLICATIONS

*These documents are distributed by the National Technical Information Service, Springfield, Va. 22151. These documents have been announced in the Clearinghouse journal U.S. Government Research & Development Reports (USGRDR) under the indicated AD numbers.*

## SL-7 PUBLICATIONS TO DATE

SL-7-1, (SSC-238) - *Design and Installation of a Ship Response Instrumentation System Aboard the SL-7 Class Containership S.S. SEA-LAND McLEAN* by R. A. Fain. 1974. AD 780090.

SL-7-2, (SSC-239) - *Wave Loads in a Model of the SL-7 Containership Running at Oblique Headings in Regular Waves* by J. F. Dalzell and M. J. Chiocco. 1974. AD 780065.

SL-7-3, (SSC-243) - *Structural Analysis of SL-7 Containership Under Combined Loading of Vertical, Lateral and Torsional Moments Using Finite Element Techniques* by A. M. Elbatouti, D. Liu, and H. Y. Jan. 1974. AD-A002620.

SL-7-4, (SSC-246) - *Theoretical Estimates of Wave Loads on the SL-7 Containership in Regular and Irregular Seas* by P. Kaplan, T. P. Sargent, and J. Cilmi. 1974. AD-A004554.

SL-7-5, (SSC-257) - *SL-7 Instrumentation Program Background and Research Plan* by W. J. Siekierka, R. A. Johnson, and CDR C. S. Loosmore, USCG. 1976. AD-A021337.

SL-7-6, (SSC-259) - *Verification of the Rigid Vinyl Modeling Techniques: The SL-7 Structure* by J. L. Rodd. 1976. AD-A025717.

SL-7-7, (SSC-263) - *Static Structural Calibration of Ship Response Instrumentation System Aboard the SEA-LAND McLEAN* by R. R. Boentgen and J. W. Wheaton. 1976. AD-A031527.

SL-7-8; (SSC-264) - *First Season Results from Ship Response Instrumentation Aboard the SL-7 Class Containership S.S. SEA-LAND McLEAN in North Atlantic Service* by R. R. Boentgen, R. A. Fain, and J. W. Wheaton. 1976. AD-A039752.

SL-7-9, *Second Season Results from Ship Response Instrumentation Aboard the SL-7 Class Containership S. S. SEA-LAND McLEAN in North Atlantic Service* by J. W. Wheaton and R. R. Boentgen. 1976. AD-A034162.

SL-7-10, *Third Season Results from Ship Response Instrumentation Aboard the SL-7 Class Containership S. S. SEA-LAND McLEAN in North Atlantic Service* by R. R. Boentgen. 1976. AD-A034175.

SL-7-11, (SSC-269) - *Structural Tests of SL-7 Ship Model* by W. C. Webster and H. G. Payer. 1977. AD-A047117.

SL-7-12,(SSC-271) - *A Correlation Study of SL-7 Containership Loads and Motions - Model Tests and Computer Simulation* by P. Kaplan, T. P. Sargent, and M. Silbert. 1977. AD-A049349.

SL-7-13, *A Report on Shipboard Waveheight Radar System* by D. Chen and D. Hammond. 1978. AD-A053379.

SL-7-14, (SSC-277) - *Original Radar and Standard Tucker Wavemeter SL-7 Containership Data Reduction and Correlation Sample* by J. F. Dalzell. 1978.

SL-7-15, (SSC-278) - *Wavemeter Data Reduction Method and Initial Data for the SL-7 Containership* by J. F. Dalzell. 1978.

SL-7-16, *Radar and Tucker Wavemeter Data from S. S. SEA-LAND McLEAN - Voyage 32* by J. F. Dalzell. 1978.

SL-7-17, *Radar and Tucker Wavemeter Data from S. S. SEA-LAND McLEAN - Voyage 33* by J. F. Dalzell. 1978.

SL-7-18, *Radar and Tucker Wavemeter Data from S. S. SEA-LAND McLEAN - Voyage 34* by J. F. Dalzell. 1978.

SL-7-19, *Radar and Tucker Wavemeter Data from S. S. SEA-LAND McLEAN - Voyages 35 and 36E* by J. F. Dalzell. 1978.

SL-7-20, (SSC-279) - *Modified Radar and Standard Tucker Wavemeter SL-7 Containership Data* by J. F. Dalzell. 1978.

SL-7-21, *Radar and Tucker Wavemeter Data from S. S. SEA-LAND McLEAN - Voyage 60* by J. F. Dalzell. 1978.

SL-7-22, *Radar and Tucker Wavemeter Data from S. S. SEA-LAND McLEAN - Voyage 61* by J. F. Dalzell. 1978.

SL-7-23, (SSC-280) - *Results and Evaluation of the SL-7 Containership Radar and Tucker Wavemeter Data* by J. F. Dalzell. 1978.